Holocene glacier readvances on the Fildes Peninsula, King George Island (Isla 25 de Mayo), NW Antarctic Peninsula

Pablo Heredia Barión[1,2,3], Stephen J. Roberts[4*], Cornelia Spiegel[2], Steven A. Binnie[5], Lukas Wacker[6], Joanna Davies[7], Imogen Gabriel[8], Vivienne J. Jones[7], Simon Blockley[8], Emma J. Pearson[9], Louise Foster[4,9], Sarah J. Davies[10], Thomas P. Roland[11], Emma P. Hocking[12], Michael J. Bentley[13], Dominic A. Hodgson[4,13], Chris L. Hayward[14], Robert D. McCulloch[15], Jorge A. Strelin[3, 16], Gerhard Kuhn[1]

[1]Alfred-Wegener-Institut Helmholtz-Zentrum für Polar- und Meeresforschung, Geosciences Division, Am Alten Hafen 26, 27568 Bremerhaven, Germany.
[2]University of Bremen, Department of Geosciences, Klagenfurterstr. 2–4, 28359 Bremen, Germany.
[3]Centro de Investigaciones en Ciencias de la Tierra (CONICET-UNC), Vélez Sársfield 1611, X5016GCA, Córdoba, Argentina.
[4]British Antarctic Survey (BAS), Natural Environmental Research Council (NERC), High Cross, Madingley Road, Cambridge CB3 0ET, UK.
[5]Institute for Geology und Mineralogy, University of Cologne, Zuelpicher Str. 49b, Cologne D-50674, Germany.
[6]ETH Zürich, Laboratory of Ion Beam Physics, Schafmattstrasse 20, CH-8093 Zürich, Switzerland.
[7]ECRC Dept. of Geography, University College London, North West Wing, Gower St, London WC1E 6BT, UK.
[8]Dept. of Geography, Royal Holloway, University of London, Egham, Surrey, TW20 OEX, UK.
[9]School of Geography, Politics and Sociology, Newcastle University, Newcastle-upon-Tyne, NE1 7RU, UK.
[10]Aberystwyth University, Department of Geography and Earth Sciences, Aberystwyth, SY23 3DB, UK.
[11]Department of Geography, University of Exeter, Exeter EX4 4RJ, UK.
[12]Department of Geography, Northumbria University, Ellison Building, Newcastle-upon-Tyne NE1 8ST, UK.
[13]Department of Geography, Durham University, Durham DH1 3LE, UK.
[14]School of Geosciences, Grant Institute, University of Edinburgh, The King's Buildings, James Hutton Road, Edinburgh EH9 3FE.
[15]Centro de Investigación en Ecosistemas de la Patagonia, Coyhaique, Aysén, Chile.
[16]Instituto Antártico Argentino, Convenio MREC - Universidad Nacional de Córdoba, Vélez Sársfield 1611, X5016GCA, Córdoba, Argentina.

*Corresponding author: Stephen J. Roberts (sjro@bas.ac.uk) ORCiD: 0000-0003-3407-9127

Abstract

The timing of mid–late Holocene deglaciation and glacier readvances on the South Shetland Islands, northern Antarctic Peninsula has been long debated. We used a combined geomorphological, chronological, and palaeolimnological approach to develop a new readvance model for the Bellingshausen Ice Cap (BIC) on the Fildes Peninsula, King George Island/Isla 25 de Mayo, South Shetland Islands, NW Antarctic Peninsula. Results show that retreat to within present-day limits occurred by c. 6 ka, as spring/summer insolation at 62 °S peaked. Probability density analysis of new and previously published chronological data (n=80) from across Fildes Peninsula and King George Island identified up to eight probability 'gaps' when glacier readvances might have occurred: 1) a well-defined readvance (with a marine transgression) between c. 7.4–6.6 ka cal BP; 2–5) four possible readvances between c. 5.3–4.8 ka cal BP, 4.5–3.9 ka cal BP, 3.3–3.0 ka cal BP and/or 2.6–2.2 ka cal BP; 6) a well-defined readvance at 1.7–1.3 ka; 7–8) well-defined readvances between c. 1.3–0.7 and after <0.7 ka cal BP. Mid-late Holocene readvances of the BIC on the Fildes Peninsula were limited to within or around the current ice margin. Prior to c. 5 ka cal BP, readvances were initiated during phases of reduced global solar irradiance, with colder and more humid negative Southern Annular Mode (SAM)-like conditions. After c. 5 ka, a declining trend in insolation at 62 °S led to persistently colder/ wetter and more negative SAM-like conditions that likely drove late Holocene readvances.

2

Introduction

Field-based reconstructions of Antarctic ice sheet and ice cap deglaciation and after the Last Glacial Maximum (c. 26–18 ka) into the Holocene are important components of ice sheet models that examine the impact of future ice-melt on rates of regional-global sea-level change (Sugden and Clapperton, 1977; Ó Cofaigh et al., 2014; Lindow et al., 2014; Simms et al., 2019; Kaplan et al., 2020; Nývlt et al., 2020; Oliva et al., 2020). Ice-marginal and ice-free coastal areas on the Antarctic Peninsula (AP) and South Shetland Islands (SSI) contain an abundance of readily accessible morphostratigraphic features (e.g., raised beaches), lake sediment records, and glacially transported erratics which can be used to constrain past glacier dynamics.

Despite numerous studies, the timing of early-mid Holocene deglaciation and the number, timing and extent of mid–late Holocene glacier readvances on South Shetland Islands and across the northern Antarctic Peninsula (NAP) remain debated (Hall, 2007; Hall, 2009; Simms et al., 2011; Watcham et al., 2011; Simms et al., 2012; Ó Cofaigh et al., 2014; Emslie et al., 2019; Oliva et al., 2019). The glacial history of the Fildes Peninsula in the south-west of King George Island (KGI)/Isla 25 de Mayo, the largest of the South Shetland Islands (Figure 1) has been determined by cosmogenic isotope exposure dating of bedrock, radiocarbon and optically stimulated luminescence (OSL) dating of organic remains embedded in raised beaches and moraines of the c. 1250 km^2 Bellingshausen Ice Cap (BIC; also known as the Collins Ice Cap), as well as radiocarbon ages from lake sediments and terrestrial stratigraphic sequences overlying coarse grained sediments and diamictons (Figure 1) (Sugden and John, 1973; Pallàs et al., 1997; Bentley et al., 2005; Seong et al., 2008; Hall, 2010; Watcham et al., 2011; Simms et al., 2012; 2021).
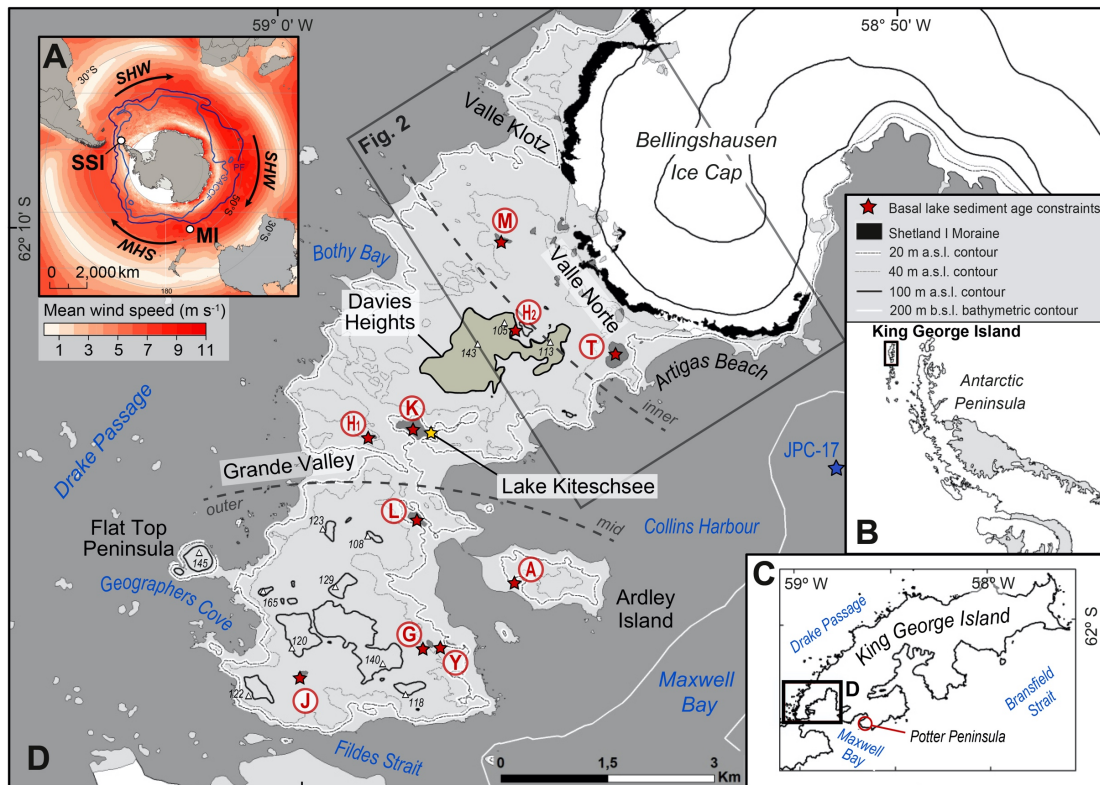
3

Figure 1. Geographic location of the study area. A) Location of the South Shetland Islands (SSI), currently south of the core Southern Hemisphere westerly Wind (SHW) belt. MI is Macquarie Island, located within the core SHW belt. B) Location of King George Island (KGI), South Shetland Islands on the north-western Antarctic Peninsula. C) KGI is framed by the Drake Passage and the Bransfield Strait. Box marks the position of Fildes Peninsula. D) Map of Fildes Peninsula showing minimum ages (a cal BP) for the onset of lake and offshore sedimentation. The Fildes Strait separates the Fildes Peninsula from Nelson Island, with Maxwell Bay to the east, and the open waters of the Drake Passage on its west coast. Lake record basal deglaciation ages (a cal BP ± 2σ), updated to Sh20/Marine20 for this study are as follows: Outer: J-Jurasee Lake (9,750±780 a cal BP) (Mäusbacher et al., 1989); Y-Yanou Lake (10,830±340 a cal BP) (Watcham et al., 2011; Roberts et al. 2017; G-Gaoshan Lake (7,250±120 a cal BP) (Watcham et al., 2011); A-Ardley Lake (8,310±120 a cal BP) (Watcham et al., 2011; Roberts et al., 2017); L-Long Lake (>6,480±180 a cal BP) (Yoon et al., 2006; Watcham et al., 2011; Mid: Marine core JPC-17 (5,800 a cal BP) (Simms et al., 2011); K-Kiteschsee Lake (>7,300±120 a cal BP) (this study and Mäusbacher, 1991); H_1-Hotel Lake (6,960±150 a cal BP) (Tatur et al., 1999); H_2-Hochlandsee Lake (6,150±400 a cal BP) (Mäusbacher, 1991); Inner: T-Tiefersee (Profound) Lake (6,120±360 a cal BP); M-Mondsee Lake (8,000±480 a cal BP) (Schmidt et al., 1990). Contour lines: Antarctic Digital Database (http://www.add.scar.org/home/add7); bathymetry: GEBCO (Weatherall et al., 2015); spot heights (white triangles): Servicio Geográfico Militar de Uruguay; asterisks indicate new data in this study.

Isolation basins raised beaches and marine abrasion terraces used to constrain glacio-isostatic

adjustment (GIA) (uplift) and changes in relative sea level (RSL) are often regarded as the most

4

reliable datasets for establishing deglacial unloading and reloading associated with glacier readvance(s) (Bentley et al., 2005; Johnson et al., 2022). The SSI have a complex geological structure due to their position above a former subduction zone and adjacent to an extending basin in Bransfield Strait (Christeson et al., 2003) and variations in elastic strength and underlying viscosity have not yet been captured in glacio-isostatic adjustment (GIA) models (van der Wal et al., 2015). Consequently, RSL data are more complex for the SSI than for other locations across Antarctica, and several different RSL curves have been suggested (Pallàs et al., 1997; Bentley et al., 2005; Hall, 2010; Roberts et al., 2011; Watcham et al., 2011; Simms et al., 2012; 2021; Johnson et al., 2021). While some GIA models (e.g., Whitehouse et al., 2012) infer changes in ice loading consistent with RSL reconstructions based on well-dated isolation basin records from Fildes Peninsula (Watcham et al., 2011; Roberts et al., 2017), the coarse spatial resolution of GIA models means they are not currently able to capture smaller scale isostatic responses and RSL reversals implied by field data (Simms et al., 2012; Whitehouse et al., 2012; Simms et al., 2019; 2021; Johnson et al., 2021). Spatially-variable responses of glacio-isostatic uplift are thought to have occurred across the SSI and AP during the mid-late Holocene (Fretwell et al., 2010; Zurbuchen and Simms, 2019), necessitating new approaches to data collection and analysis.

Here, we examine the deglaciation and redavance history of the BIC outlet of the Fildes Peninsula using a novel combined morphostratigraphic-chronological-palaeolimnological-statistical approach to provide new constraints on glacier readvances across the Fildes Peninsula during the mid–late Holocene. As sufficiently large local-regional chronological datasets constraining glacier activity now exist for KGI and the SSI (i.e., ~n>50), 95% probability density phase analysis was used to identify 'probability gaps' in chronological data which constrain when glacier readvances from the BIC on the Fildes Peninsula, could have occurred. By comparing evidence for BIC readvances with those from across the SSI, we test

5

the hypothesis that Holocene retreat of the BIC was discontinuous, and interrupted by more than one glacial readvance during the mid–late Holocene, rather than a continuous deglacial process. We also examine possible driving mechanisms for deglaciation and readvance(s) on the SSI and the NAP.

To achieve our aims, first we obtained minimum ages for deglaciation from new Berylium-10 (^{10}Be) cosmogenic isotope exposure dating of granitic erratics deposited at ~40–35 m a.s.l. deposited as glaciers retreated from offshore LGM limits across the NW marine platform and BIC foreland (Figure 1). Second, we obtained new radiocarbon ages from terrestrial and marine macrofossils that were living on the BIC foreland on Fildes Peninsula before glacier readvance embedded them into moraines; these data represent maximum ages of glacier advance. Third, we undertook detailed multi-proxy analyses on a new lake sediment core extracted from Kiteschee Lake (62° 11'36.55''S, 58° 57'59.93''W) and compared these results to basal ages and multiproxy data from previously published lake records to determine when deglaciation occurred in different sectors of the Fildes Peninsula (inner, mid, outer; Figure 1) and if mid-late Holocene readvance(s) impacted on lake ecosystems. Overall, we identified eight periods in the mid-late Holocene when glacier readvances could have occurred.

Regional setting & Study area

Climate setting

The SSI archipelago is a ~230 km long, ~35 km wide active volcanic arc of 11 major islands, with Fildes Peninsula located at ~62° S, 58–59° W and ~130 km northwest of the Antarctic Peninsula (Figure 1B). The SSI are located south of the Polar Front at 50–55°S, where the southern limb of the Southern Hemisphere Westerly winds (SHW) belt converges with the polar cell (Figure 1A). Sandwiched between the high pressure subtropic and Antarctic anticyclones, the SSI island chain has a milder and more humid (wetter) maritime climate than

the Antarctic continent with more than ~1000 mm yr^{-1} of precipitation, which maintained a stable to slightly negative glacier mass balance for the BIC and an equilibrium altitude (ELA) of ~ 150 m a.s.l. between 1970–90 CE (Turner et al., 2002; Bentley et al., 2009; Falk et al., 2018). Intense cyclonic activity through the Drake Passage, associated with the SHW to the north, and the low-pressure circumpolar belt to the south (~66°S) means the SSI experience cloud cover for ~80% of the year (King and Turner, 1997; Bañón et al., 2013).

The annual mean air temperature on KGI between 1948 and 2011 CE was -2.5 ºC (Kejna et al., 2013). Mean annual, summer and winter air temperatures at the Russian Bellingshausen Station, Fildes Peninsula, between 1968–2015 CE (Olivia et al., 2017) and (1968–2021 CE) (BAS READER project – Reference Antarctic Data for Environmental Research; Turner et al., 2004) were -2.3°C (-2.3±3.1°C), 1.1°C (1.1±0.8°C) and -6.1°C (-5.9±1.7°C), respectively, with mean summer air temperatures above zero and snow free conditions (at sea level) up to four months between December and March (Michel et al., 2014). Mean annual, summer and winter wind velocities recorded at Bellingshausen (1968–2021 CE) were 26.5±3.5 km h^{-1}, 23.8±2.2 km h^{-1}, 27.3±3.2 km h^{-1}, respectively. Persistent ~100 km h^{-1} storms are common across the SSI, with wind directions predominantly SW/W/NW to NE/E/SE (34% W/NW to E/SE), but rarely along the NE-SW axis (ref)

A warming trend across the Antarctic Peninsula and SSI between the 1950 and 1999 CE drove increased rates of glacier retreat, ice-shelf collapse (Vaughan et al., 2003; Meredith and King, 2005) and elevated the ELA on the SSI to above 200 m a.s.l. (Falk et al. 2018). Similar to most other stations on the AP and SSI, temperature data from the Bellingshausen Station exhibit decadal scale variability, which has been linked to the El Niño Southern Oscillation (ENSO) (Oliva et al., 2017). Warming initiated ~5 years prior to El Niño in 1982–3 CE and 1997–8 CE was followed by a cooling trend to 2015 CE and a return to a warming trend between 2015-21

7

CE (Figure1E). The shift to a cooling trend between 1999–2015 CE has been observed across NAP, with recent record summer temperatures on the northeastern AP attributed to an enhanced fohn effect (Turner et al., 2016; Oliva et al., 2017).

 Climate variability on the SSI is controlled by the interaction between (spring/summer) insolation and the position and intensity of the SHW, modulated by changes in the Southern Annular Mode (SAM) (Moy et al., 2008; Bentley et al., 2009; Lamy et al., 2010; Varma et al., 2012) (Figure 1A). The SAM is the primary mode of annual to centennial scale variability in atmospheric circulation in the Southern Ocean (Marshall, 2007). It reflects the zonal mean sea level pressure difference between Antarctica (>65°S) and the mid latitudes (40°S). The SAM index is a measure of the longitudinal mean SHW strength and positive SAM phases are associated lower pressure at higher latitudes and more poleward focussed SHW. In general, stronger, and more poleward-shifted SHW are the millennial-scale expression of decadal-centennial warming and more positive SAM-like conditions (Charman et al., 2018; Perren et al., 2020). Seasonally over the NAP and SSI, positive SAM phases are characterised by stronger Westerlies in summer and stronger Easterlies in winter (Martin et al., 2021). Conversely, negative SAM phases are characterised by colder and more humid conditions on the NAP, SSI and sub-Antarctic islands (Reynhout et al., 2019; Kaplan et al., 2020; Verfaillie et al., 2021). Since 1957 CE, the longer-term pattern of interannual variability in the SAM has been altered by the ozone hole over Antarctica, which, combined with increased greenhouse gases and global temperature have forced a more positive trend in the SAM and enhanced ENSO (Marshall, 2007).

Geology and Glaciation

King George Island, the largest of the South Shetland Islands, has been subdivided into three tectonic regions: the Fildes Block (Fildes Peninsula), Barton Horst (Barton and Weaver

Peninsulas) and the Warszawa Block (Potter Peninsula) (Smellie et al., 1984; Watcham et al., 2011). Covering an area of 38 km^2, the Fildes Peninsula is the largest ice-free area on the South Shetland Islands. It is composed of predominately andesitic and basaltic lava bedrock, with some interbedded terrestrial sediments, including shales and conglomerates (Smellie et al., 1984). Most of the Bellingshausen Ice Cap (BIC) foreland was glaciated during the Last Glacial Maximum (pre-LGM) and consists of raised marine platforms up to 180 m a.s.l. of pre-LGM age and formed by basic volcanic rocks of Late Cretaceous to Paleogene-age (John and Sugden, 1971) . The eastern coastline of the Fildes Peninsula is indented with coves, while the western coast is characterized by sheer sea cliffs and stacks (Hall, 2003).

The elevated island interiors of the SSI are characterized by numerous ice caps and permanent snowfields and the coastal fringes are some of the most extensive ice-free and permafrost areas in Antarctica (Braun et al., 2004; Ó Cofaigh et al., 2014) (Figure 1B). Chlorine-36 (^{36}Cl) exposure ages from glacially striated bedrock on nearby Barton Peninsula from above c. 50 m a.s.l. show that progressive ice thinning on KGI, South Shetland Islands started c. 15,000 years ago (Seong et al., 2009). On the northern half of Fildes Peninsula, the BIC is bounded by prominent moraines, referred to as Shetland I (Hall, 2007). A prominent, and largely featureless, marine platform of pre-Holocene age at c. 40-35 m a.s.l. on north-western Fildes Peninsula, is more than 7 km long and 1 km wide (John and Sugden, 1971) (Figure 1). This feature is flat to gently undulating, seaward sloping with a limited number of undated granite erratics on its surface (Barsch and Mäusbacher, 1986; Hall, 2003). As far as we are aware, granite erratics on the South Shetland Islands and BIC foreland have not been previously dated using the cosmogenic exposure dating method.

Basal lacustrine sedimentary sequences in the mid-southern part of Fildes Peninsula have been dated to c. 10 ka cal BP (e.g., Jurasee Lake (Mäusbacher et al., 1989)) and were formed in

9

over-deepened glacial basins. Several former marine embayments with basal sediment ages of up to c. 12 ka cal BP (Watcham et al., 2011) were transformed into freshwater (isolation) basins when the rate of isostatic uplift outpaced the declining rate of sea level rise during the early Holocene (Watcham et al., 2011). Radiocarbon ages obtained from marine-terrestrial transition sediments and raised beaches have been used to reconstruct past changes in local RSL at several sites across the South Shetland Islands. These indicate that the thickest part of the South Shetland Islands ice cap was probably centred on the now ice-free area of Fildes Peninsula during the LGM (Watcham et al., 2011). The South Shetland Islands ice cap was possibly separated from the Antarctic Peninsula Ice Sheet by the Bransfield Marginal Basin during the LGM, but more likely became independent during the Lateglacial–Interglacial transition (c. 15–12 ka) (John and Sugden, 1971; Fretwell et al., 2010; Watcham et al., 2011; Ó Cofaigh et al., 2014).

Kiteschsee lake, in the eastern-central region of the Fildes Peninsula, is c. 550 m from the east coast and approximately 2.6 km from the margin of the BIC (Figure 1D, 2B). It is close to the Davies Heights (>100 m a.s.l.), a previously glaciated part of the former raised marine platform in the mid-central area of Fildes Peninsula, which supplies meltwater directly into the eastern end of the lake (Figure 1). A well-defined Holocene marine high-stand of 18–15 m a.s.l. occurred on Fildes Peninsula between c. 8 and 7 ka (Mäusbacher et al., 1989; Watcham et al., 2011). Marine sediments at the base of a previously studied sedimentary record from Kiteschsee Lake (Mäusbacher et al., 1989) show that much of the low-altitude central area of Fildes Peninsula remained below sea-level until c. 7–6 ka (Mäusbacher et al., 1989). Since Kiteschsee Lake is at c. 15 m a.s.l., it was a terrestrial lake basin from 6 ka cal BP onwards (Mäusbacher, 1991; Watcham et al., 2011).

Methods

10

Cosmogenic nuclide surface exposure dating of erratics

The cosmogenic isotope concentration accumulated in a superficial rock sample is proportional to the length of time exposed to cosmic rays at the Earth's surface (Balco, 2011). The cosmogenic exposure age produced depends on the production rate, which reflects the concentration of cosmogenic isotopes produced each year per gram of the relevant mineral. This varies spatially and temporally due to variations in atmospheric depth and geomagnetic field effects (Lifton, 2016). Although ^{10}Be has the most well-constrained production rate and can be measured at low concentrations (Balco, 2011), glacially striated and quartz-rich, granitic bedrock and erratics required for ^{10}Be isotope cosmogenic analysis are rare in the basaltic-andesitic volcanic-arc environment of the South Shetland Islands, compared with other regions of Antarctica. All of the limited number of large boulders >50 cm in diameter on the NW BIC glacial foreland were surveyed and classified. Differential GPS (dGPS; WGS84 ellipsoid) data for erratic boulders was obtained using a GPS Trimble Pathfinder ProXH. As geodetic reference, we used the landmark DALL 66019M002 (S62°14′16.335″, W58°39′52.364″, ellipsoidal height 39.376 m) at the Argentine Carlini base, c. 17 km from the sampled erratics. Post-processed uncertainties for the samples were less than 0.1 m in altitude and in the horizontal. Only three large granitic boulders not incorporated into solifluction planes were considered suitable for cosmogenic nuclide exposure dating with ^{10}Be. The sampled erratics showed no signs of significant erosion (Table 1) and their size meant it is very unlikely they had been overturned. Post-depositional movement was minimized by collecting samples away from slopes or cliffs. Samples were taken with a hammer and chisel, removing the upper few centimetres of sub-horizontally exposed surfaces (Figure 2C). The angle to the skyline from each sample was measured to calculate topographic shielding (Balco et al., 2008). Surface shielding due to snow cover was minimised by sampling from wind-exposed localities (cf. Johnson et al., 2012, 2017, 2020; Glasser et al., 2014; Lindow et al., 2014).
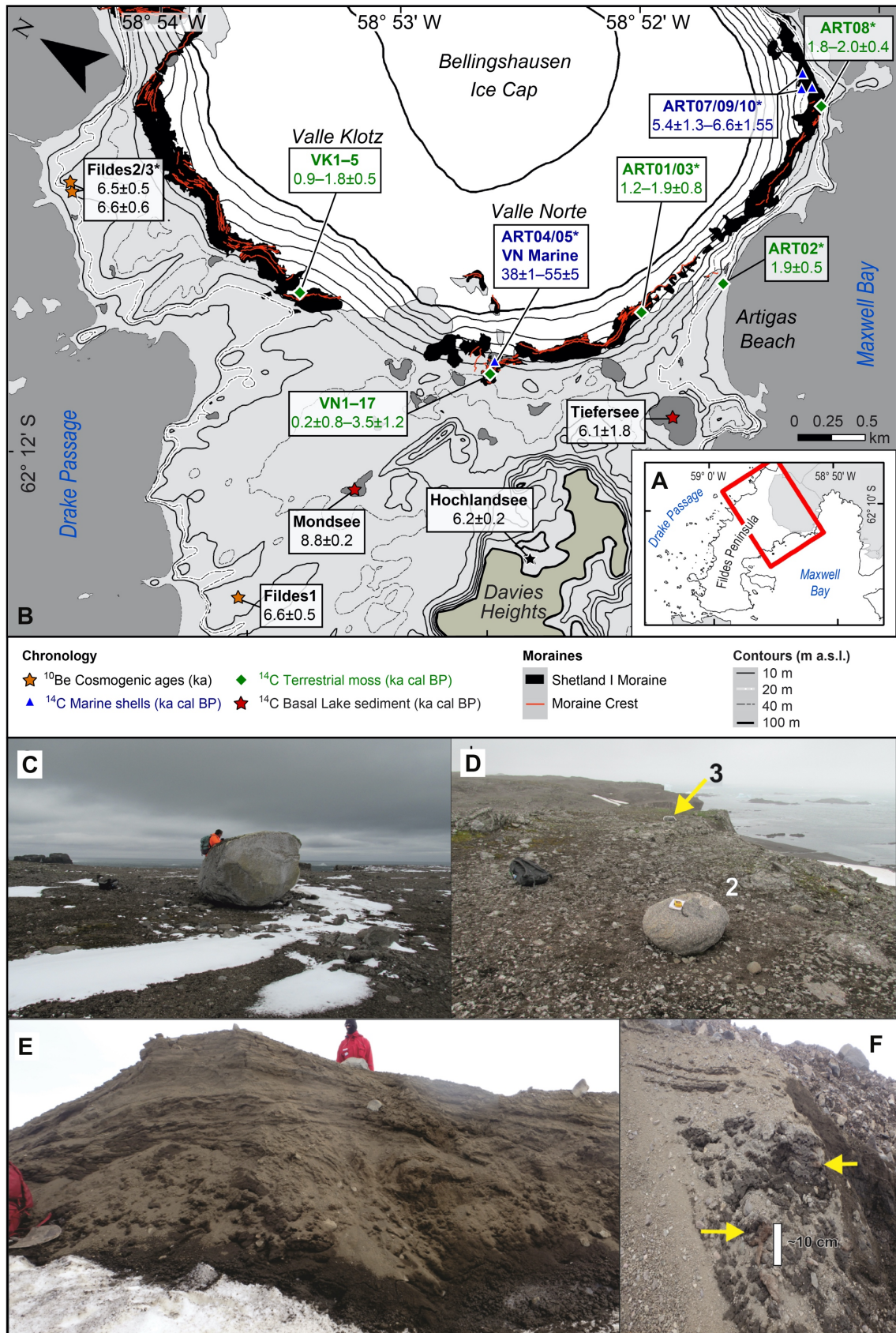
11

Figure 2. A–B) Map showing the position of cosmogenic [10]Be exposure ages of sampled erratics (orange stars) and calibrated radiocarbon ages of organic remains in the Shetland I moraine (black shading) and minimum ages of the onset of lake sedimentation (red stars). Inset map shows the area where the study sites are located (red box) BIC is Bellingshausen Ice Cap,

12

mcs = marine carbonate shells, m= mosses, ls = lake sediments. C–F) Field photographs showing the erratics sampled on the NW marine platform for terrestrial cosmogenic nuclide exposure age dating and terrestrial sediments preserved within the Shetland I moraine. C) Fildes 1 and D) Fildes 2 and 3 boulders sampled for cosmogenic analysis. Boulder dimensions and locations are in Table 1. E & F) Radiocarbon dating samples from locations ART-01 and ART-03 embedded in moraine sediments (Table 2).

Laboratory analysis for [10]Be cosmogenic nuclide surface exposure dating followed the procedures of Kohl and Nishiizumi, (1992) and Binnie et al., (2015) (Supplementary Note 1). Exposure ages were calculated using version 3 of the online calculator described by Balco et al., (2008). Following standard procedures for the Antarctic Peninsula region, we used the Antarctic ("Ant") pressure flag and the scaling scheme "LSDn" (Stone, 2000; Lifton et al., 2014). We employed the scaling model "LSDn" because it derives from an improved understanding of the atmospheric particle flux and neutron spectrum (Lifton et al., 2014), as compared with other scaling schemes using empirical fits to proxy data. A rock density of 2.7 g cm^{-3} was assumed for the samples. Exposure ages are derived using the default [10]Be production rate calibration dataset (Borchers et al., 2016) in the online calculator of Balco et al (2008), however, for comparison, Table 1 also provides [10]Be ages calculated using the mid-latitude southern hemisphere New Zealand (Putnam et al., 2010) and Patagonian calibration datasets (Kaplan et al., 2011) since these are proximal to Antarctica. No snow cover or erosion rate correction was applied. Internal and external uncertainties (Balco et al., 2008) are reported and we use external uncertainties to compare new exposure ages with calibrated AMS radiocarbon ages collected in this study.

Radiocarbon dating of moraines and stratigraphic sections

Moraines adjacent to the BIC were mapped and interpreted from field observations and satellite images (DigitalGlobe, Catalogue ID: 1030010020C0C900; Google Earth, 2006 and 2011). Contour lines are derived from the Antarctic Digital Database with elevation data (±5 m) obtained from the map of Servicio Geográfico Militar de Uruguay (Instituto Antártico

13

Uruguayo, Uruguay, 1997). Radiocarbon ages from moraines and stratigraphic sections were obtained by Accelerated Mass Spectrometry (AMS) dating of marine mollusc shells, terrestrial mosses and seaweed layers embedded in sediments and represent maximum ages for BIC glacier readvance (Table 2). To reduce the risk of contamination with modern material, all samples for radiocarbon dating were taken from fresh and previously cleaned outcrops or sediment cores, packed in zip-lock plastic bags and stored at 4°C. Sample preparation prior to radiocarbon dating analysis was undertaken at the Alfred Wegener Institute Helmholtz Centre for Polar and Marine Research and the British Antarctic Survey. Sample measurements and corrections for $^{13}C/^{12}C$ ratio and calculation of Conventional Radiocarbon Ages were undertaken by ETH Zürich and SUERC, Scotland.

Calibration of radiocarbon ages from marine samples was undertaken in Oxcal v. 4.4 using the Marine20 calibration curve (Bronk Ramsey, 2009; Heaton et al., 2020), and a newly recalculated local marine reservoir age offset (ΔR) of 666±76 ^{14}C years (Heaton et al., 2020), which represents the weighted mean ΔR of four radiocarbon-dated marine samples collected prior to 1950 CE from the northern Antarctic Peninsula and Signy Island in the CALIB online Marine20 database (http://calib.org/marine/) (Table 2, S3; Supplementary Note 1for details). Terrestrial samples, Kiteschsee Lake samples and previously published data from Yanou Lake (Roberts et al., 2017), were (re)calibrated using the Southern Hemisphere SHCal20 calibration curve in Oxcal v. 4.4 (Hogg et al., 2020). There were no significant statistical differences (i.e., beyond two-sigma error ranges) between Holocene radiocarbon ages calibrated using the SHCal13/Marine13 (Hogg et al., 2013) and the ShCal20/Marine20 curves (ShCal13 vs 20: n=19, mean difference ± 1σ = -4±8 years; Marine: n=8, mean difference ± 1σ = -45±8 years), hence, comparisons to published data and age models calibrated using the SHCal13 and Marine13 curves remain valid.

Sample ID	AMS ID	Latitude (°S) Longitude (°W)	Altitude (m amsl)	Boulder dimension (L x W x H) (m)	Sample thickness (cm)	^{10}Be concentration (atoms g^{-1})	^{10}Be concentration 1σ (atoms g^{-1})	^{10}Be age (yr) (Ww) ± 1σ int (ext) error	^{10}Be age (yr) (Pt) ± 1σ ext. error	^{10}Be age (yr) (Kp) ± 1σ ext. error	Context
Fildes1	s08808	62° 10' 2.34" S 58° 57' 45.97" W	43	2.65 x 2.10 x 1.98	1.4	37.1 x 10^3	1.9 x 10^3	6630 ± 340 (520)	6640 ± 350	6830 ± 660	Erratic (retreat)
Fildes2	s08809	62° 08' 43.65" S 58° 55' 35.96" W	40	0.87 x 0.71 x 0.35	1.2	36.4 x 10^3	2.0 x 10^3	6510 ± 350 (520)	6530 ± 370	6710 ± 660	Erratic (retreat)
Fildes3	s08810	62° 08' 43.97" S 58° 55' 37.18" W	39	0.74 x 0.62 x 0.26	1.2	36.9 x 10^3	2.2 x 10^3	6610 ± 390 (550)	6630 ± 400	6810 ± 680	Erratic (retreat)

Table 1. Cosmogenic surface exposure dating results. In v.3 of the online calculator of Balco et al. (2008), we assumed zero erosion, used the AMS standard flag 07KNSTD, an "ant" elevation pressure flag and a density of 2.7 g cm^{-2}. A shielding correction of 0.9999 was applied to all samples as the value is the same for all. Calculations of ^{10}Be exposure ages using the global (Ww) "LSDn" scaling (Lifton et al., 2014), the New Zealand-Macaulay (Pt) (Putnam et al., 2010), and the Patagonia calibration dataset (KP) (Kaplan et al., 2011). int: Internal error; ext: External error; ages have been rounded to the nearest 10 years. Lm production rate scaling from the online calculator (Balco et al., 2008) would give ages that are around 2% older, and thus within the uncertainties on the ages we report using LSDn. For the batch of three samples, the laboratory blank used to correct ^{10}Be concentrations was 2.06 x10^{-15} ± 3.71x10^{-16}, amounting to a maximum background correction of less than 6% of the total ^{10}Be atoms measured.

Kiteschsee Lake record

Lithology and geochemistry: We undertook multi-proxy analyses (diatom, grain size, geochemical and sedimentological analysis) on a 77 cm-long sediment record extracted from the flat-bottomed eastern basin depocentre of Kiteschsee Lake (Figure 4, S1–3) and compared data obtained with published lake records from Fildes Peninsula. High resolution X-ray fluorescence (ITRAX) core scanning (XRF-CS) of bulk, wet sediment was performed at contiguous 0.02 cm (200 µm) intervals following established procedures outlined in Davies et al. (2015) and Roberts et al. (2017) (see Supplementary Materials for further details).

Chronology: A chronology for the Kiteschsee Lake sediment record was based on two aquatic moss ages, six bulk sediment AMS radiocarbon ages, and four tephra correlation ages and established using a Bayesian age-depth Markov Chain Monte Carlo (MCMC) method in BACON v. 2.5 in R (Blaauw and Christen, 2011). Volcanic glass-shard counts and electron probe microanalysis (EPMA) data were used to improve the final age-depth model (Blockley et al., 2005; Roberts et al., 2017) (Supplementary Material). Initial model runs were fine-tuned by the inclusion of radiocarbon ages from aquatic moss in the nearby Yanou Lake record immediately below and above the 'T5', between the 'T3a' and 'T3b' tephra layers, and immediately below the 'T1a' (Figure 4B, Table S1; Supplementary Material for details). All measured radiocarbon ages were included in age-depth models and the SHCal20 calibration curve used (Hogg et al., 2020). Reporting of radiocarbon data and age-depth modelling parameters follows recommendations in (Lacourse and Gajewski, 2020). Sample thicknesses were 0.5 cm or 1 cm and no zero-depth surface age was set in the age-depth model. Runn settings and priors are described in Supplementary Note 2 and Figure S4. Modelled ages and errors were derived from the MCMC 'best-fit' weighted mean ages from the BACON age-depth model. Calibrated and modelled radiocarbon ages have been rounded to the nearest 10

years in Table 2, with two-sigma calibrated ages or 95% confidence age-depth model age ranges shown and quoted in the text. Calibrated ages in the text have been rounded to the nearest hundred years in the text to reflect realistic total (internal and external) uncertainties in radiocarbon dating.

Diatom analysis: Since the early Holocene isolation history of Kiteschsee Lake is well-established (Mäusbacher et al., 1989), and diatom smear-slide screening tests revealed that samples from 77–47 cm depth had very low diatom concentrations, quantitative analysis focussed on reconstructing high-resolution diatom compositional changes in the uppermost 47 cm (late Holocene) where diatom preservation was sufficient for meaningful environmental interpretation (Figure 4). Quantitative diatom counting and analysis was undertaken at 1–2 cm intervals on sediments between 47 cm and 5 cm depth (3,680 – -63 a cal BP) and related to μ-XRF data using Principal Component Analysis (PCA) (Figure S10, Supplementary Note 2 for details). Diatom compositional turnover (β-diversity in Figure 4, 5) was estimated down-core using Detrended Canonical Correspondence Analysis (DCCA) for the most abundant diatoms (>2%). To infer changes in chlorophyll-a shown in Figure 4, we applied the diatom-chlorophyll-a training set developed for the Antarctic Peninsula using data from 61 lakes (Jones and Juggins, 1995). Diatom-based transfer functions were applied in C2 (Juggins, 2007) using simple weighted averaging (WA) and weighted partial least squares (WA-PLS) algorithms. The WA-Inverse transfer function was chosen to reconstruct chlorophyll-a as the RMSE, and average bias were low and displayed a strong relationship (R^2) between measured and diatom-inferred chlorophyll-a (Supplementary Note 2 for details). Constrained cluster analysis (CONISS) with broken stick analysis was applied to square root transformed datasets using R packages Vegan and Rioja to define a significant number of lithofacies units and diatom zones and their boundary positions (Juggins, 2007; Juggins, 2012; Oksanen, 2014).

17

Glacier readvances and retreat data compilation and analysis

New and published chronological data constraining Holocene glacier readvances from the Fildes Peninsula (n=43), Potter Peninsula (n=29), and KGI (n=76) were compiled and a non-parametric phase model (i.e., a probabilistic version of the Oxcal SUM command) was applied to each dataset using the Bchron v. 4.7.6 in R (Haslett and Parnell, 2008; Parnell, 2021). This analysis provides a Gaussian mixture prior distribution density phase age-range estimate, at 0.68 and 0.95 probability level, constraining periods when glacier readvances could have occurred on Fildes, Potter and Barton Peninsulas KGI (FP, PP and BP in Figure 3; Table 3). Density phases produced by similar analysis of published SSI-wide data were less well-defined, likely reflecting local glacier influences and larger errors for some data, and not considered further. The Rcarbon package v. 1.4.2 (Bevan, 2021) was also used for data analysis and plotting. Mapping was undertaken in ARC-GIS and data was analysed and plotted using the Tidyverse suite of packages in R v. 4.1.0/RStudio v. 1.4.1717, Sigmaplot v. 14.0, C2 (Juggins, 2007), and MATLAB v. R2021a, with final figure layouts produced using Adobe Illustrator CC v. 2021 and CorelDRAW v. 2020.

Results

Cosmogenic nuclide surface exposure dating of erratics

The three erratic granitic boulders on the NW marine platform shown in Figure 3 gave an error-weighted mean ± internal (external) error cosmogenic surface nuclide exposure age of 6,780±220 (590) years (chi-squared, p-value 0.9718), based on the nearby Patagonian production rate (Kp in Table 1) calibration dataset, and 6,580±209 (442) years (chi-squared p-value 0.9715) based on the global calibration dataset (Ww in Table 1) (Borchers et al., 2016, both using the "LSDn" scaling scheme (Table 1). The relatively small standard deviation of the three ages of ±60 years is a favourable indicator of low analytical uncertainties but omits any systematic bias in the age related to, for example, production rate. Henceforth, we base our

discussions on the LSDn scaled age estimates (±external errors) and their weighted mean age of 6,580±440 years (Figure 2; Table 1), as reported by the v.3 of the online calculator using the global calibration dataset (Balco et al., 2008), as this provides a minimum age constraint for ice retreat coupled with a realistic estimate of external uncertainty, taking production rate uncertainty into account. However, the close agreement of the three exposure ages and the overlap between ages produced using the three different production rate calibrations datasets shown in Table 1 implies the samples had negligible pre-exposure and that they were exposed simultaneously on the NW foreland during a period of (potentially) rapid mid-Holocene glacier retreat.

Radiocarbon dating of moraines and stratigraphic sections

Twenty-six new radiocarbon ages were obtained from ten samples in the Artigas Beach–Valle Norte sections of the Shetland I moraine and its associated glaciofluvial and marine sediments (Figure 2B, 3A–C; Table 2). Shells embedded in marine sandy to silty sediments reworked into the central Valle Norte sector of the Shetland I moraine (Figure 2B) returned near infinite radiocarbon ages >40 ka cal BP, implying significant reworking of older glaciomarine deposits by the BIC (Table 2). In contrast, shells reworked into till in the Artigas Beach southern sector (Figure 2B) have a mean calibrated age range of 6.6–5.4 ka cal BP (Table 2), with two distinct 0.95 probability density age phases of 6.8–6.5 and 6.3–5.3 ka cal BP (Figure 3C; Table 3). The oldest of these ages are broadly coeval with cosmogenic exposure ages of the granite erratics (Figure 3C), which represent a minimum retreat age from the northern and central sectors of the inner BIC foreland, while the youngest are consistent with basal (deglaciation) ages from inner Fildes Peninsula lake sediment records in the Valle Norte–Artigas Beach sectors (Figure 3C, E) (Watcham et al., 2011; Roberts et al., 2017).
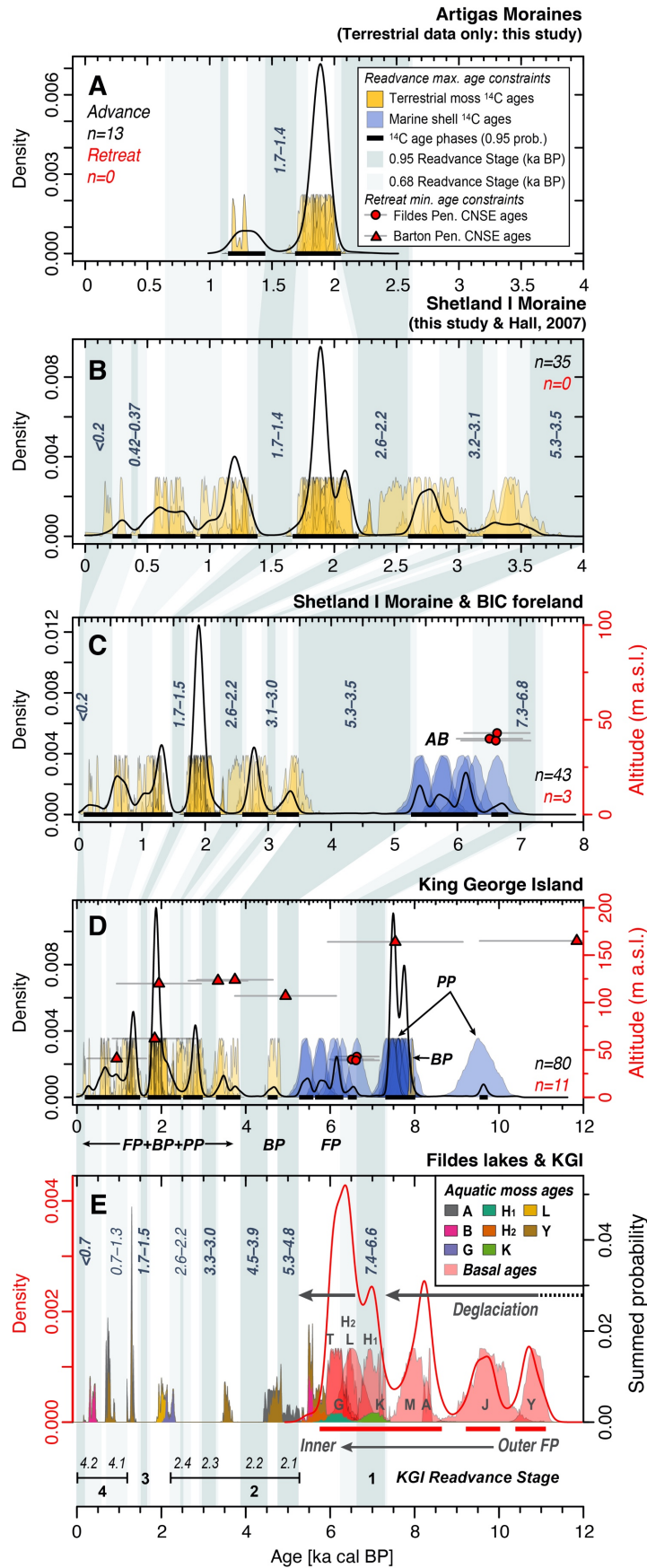
19

Figure 3. A) Radiocarbon ages and probability density phase model (black bars 95%) for terrestrial mosses dated in this study from the Artigas Beach sector moraines between 4–0 ka cal BP (i.e., sample locations ART01–03 only in Figure 2; maximum age constraints on readvance). Dark and light grey shaded zones, with 95% probability timings, indicate periods

when glacier readvances could have occurred (95% and 68% probability, respectively). B) Combined radiocarbon ages and probability density phase model for terrestrial mosses dated in this study from the Artigas Beach sector moraines and terrestrial mosses from the Valle Norte – Valle Kotz sector moraines dated by Hall (2007) between 4–0 ka cal BP; all data are maximum age constraints on readvance. C) Radiocarbon ages and probability density phase model for the Shetland I moraine 8–0 ka cal BP, consisting of terrestrial mosses and marine shells dated in this study from the Artigas Beach (AB) sector moraines, terrestrial mosses from the Valle Norte–Valle Kotz sector moraines dated by Hall (2007) (maximum age constraints on readvance). Cosmogenic exposure ages from the BIC foreland from this study are also shown (red circles; minimum age constraints on retreat) D) Probability density phase model for all maximum age constraints on glacier readvance on King George Island between 12–0 ka cal BP. Cosmogenic exposure ages from Barton Peninsula and King George Island are shown and provide minimum constraints on retreat. BP=Barton Peninsula; FP=Fildes Peninsula, PP=Potter Peninsula. E) Probability density phase model for basal deglaciation ages compared to a summed probability density profile of radiocarbon ages from aquatic moss layers in lake sediment records from Fildes Peninsula. Aquatic moss deposition represents lacustrine conditions similar to the present day. The timings of the King George Island (KGI) Readvance Stages 1–4 are also shown. The units for probability density functions used in this and other figures are ka^{-1}; all data are maximum age constraints on readvance; data sources are as described in code input datafiles.

Terrestrial moss fragments in glaciofluvial and glacial sediments from the Shetland I moraine dated in this study have mean age ranges of 2.0–1.2 ka cal BP into two well defined 95% probability density phases of 2.1–1.7 ka cal BP and 1.4–1.1 ka cal BP (n=13) (Figure 2B, 3A, D; Table 3), suggesting emplacement by limited late Holocene glacier readvances between 1.7–1.4 and/or after 1.1 ka cal BP (Figure 3A). Non-parametric 95% probability density phase modelling of all maximum age constraints from terrestrial mosses and shells emplaced in Shetland I moraines from this study and that of Hall (2007) (n=43) identified up to six possible phases when readvance of the Shetland I moraine could have occurred: 7.3–6.8 ka cal BP, 5.3–3.5 ka cal BP, 3.1–3.0 ka cal BP, 2.6–2.2 ka cal BP, 1.7–1.5 ka cal BP, <0.2 ka cal BP (Figure 3A–C; Table S3). Similar analysis of Fildes Peninsula, Potter Peninsula (Heredia Barión et al., submitted) and Barton Peninsula (Oliva et al., 2019) (n=80) data produced similar results, with seven possible overlapping periods of readvance identified: 7.4–6.6 ka cal BP, 5.3–4.8 ka cal BP, 4.5–3.9 ka cal BP, 3.3–3.0 ka cal BP, 2.6–2.2 ka cal BP and <0.2 ka cal BP (Figure 3D–E; Table S3).

| ID No.	Location Sample ID [sediment core depth]	^{14}C Lab ID	Latitude (°S)	Longitude (°W)	Altitude (m amsl)	Material dated	δ^{13}C (‰)	AMS ^{14}C age (^{14}C a)	Calibrated ages (a cal BP)						Facies dated, context, interpretation
									Max.–Min.	1σ %	Max.–Min.	2σ %	Median	Mean ± 2σ	
1	ART-03A-2015	Beta-441409	62° 10' 46.20"	58° 53' 58.34"	72	Terrestrial moss frag.	-22.7	1380 ± 30	1300–1260 / 1210–1180	37.9 / 30.4	1310–1170 / –	95.4 / –	1250	1240 ± 80	Moss in glaciofluvial sed. over 3–6; max. readvance age
2	ART-03B-2015	Beta-441410	62° 10' 46.20"	58° 53' 58.34"	72	Terrestrial moss frag.	-20.5	1380 ± 30	1300–1260 / 1210–1180	37.9 / –	1310–1170 / –	95.4 / –	1250	1240 ± 80	Moss in glaciofluvial sed. over 3–6; max. readvance age
3	ART-01A-2015	Beta-441405	62° 10' 46.20"	58° 53' 58.34"	72	Terrestrial moss frag.	-22.6	1980 ± 30	1890–1820 / 1770–1750	62.6 / 5.7	1930–1740 / –	95.4 / –	1850	1850 ± 100	Moss in glaciofluvial sediments; max. readvance age
4	ART-01B-2015	Beta-441406	62° 10' 46.20"	58° 53' 58.34"	72	Terrestrial moss frag.	-22.4	1950 ± 30	1870–1850 / 1840–1740	14.8 / 53.5	1890–1730 / –	95.4 / –	1810	1810 ± 100	Moss in glaciofluvial sediments; max. readvance age
5	ART-01A-2015 bis	Beta-441407	62° 10' 46.20"	58° 53' 58.34"	72	Terrestrial moss frag.	-19.6	1920 ± 30	1890–1820 / 1770–1750	58.0 / 10.3	1930–1740 / –	95.4 / –	1840	1830 ± 100	Moss in glaciofluvial sediments; max. readvance age
6	ART-01B-2015 bis	Beta-441408	62° 10' 46.20"	58° 53' 58.34"	72	Terrestrial moss frag.	-16.8	1940 ± 30	2000–1920 / 1910–1890	60.0 / 824.2	2010–1870 / –	95.4 / –	1950	1940 ± 80	Moss in glaciofluvial sediments; max. readvance age
7	ART-08-ar-A-2015	Beta-441411	62° 10' 54.52"	58° 51' 43.94"	16	Terrestrial moss frag.	-17.9	2030 ± 30	2010–1920 / –	68.3 / –	2050–2030 / 2020–1880	1.8 / 93.6	1960	1960 ± 80	Moss above till; max. glacial readvance age
8	ART-08-ar-B-2015	Beta-441412	62° 10' 54.52"	58° 51' 43.94"	16	Terrestrial moss frag.	-24.5	2050 ± 30	1820–1720 / –	68.3 / –	1840–1690 / 1650–1630	94.4 / 1.0	1770	1760 ± 80	Moss above till; max. glacial readvance age
9	ART-08-ab-A-2015	Beta-441413	62° 10' 54.52"	58° 51' 43.94"	16	Terrestrial moss frag.	-20.9	1870 ± 30	1830–1740	68.3	1880–1700	95.4	1790	1790 ± 80	Moss in till; max. glacial readvance age
10	ART-08-ab-B-2015	Beta-441414	62° 10' 54.52"	58° 51' 43.94"	16	Terrestrial moss frag.	-28.6	1900 ± 30	2010–1920 / –	68.3 / –	2050–2030 / 2020–1880	1.8 / 93.6	1960	1960 ± 80	Moss in till; max. glacial readvance age
11	ART-02-1A	Beta-441415	62° 10' 56.07"	58° 53' 22.15"	7	Terrestrial moss frag.	-20.5	2050 ± 30	2000–1960 / 1940–1880	24.0 / 44.2	2000–1830 / –	95.4 / –	1920	1930 ± 80	Moss in till, overlying 6-7 m amsl raised beach
12	ART-02-2A	Beta-441417	62° 10' 56.07"	58° 53' 22.15"	7	Terrestrial moss frag.	-21.9	2010 ± 30	1930–1830 / – / –	68.3 / – / –	2000–1950 / 1940–1820 / 1770–1750	12.6 / 81.6 / 1.3	1890	1890 ± 100	Moss in till, overlying 6-7 m amsl raised beach
13	ART-02-2B	Beta-441418	62° 10' 56.07"	58° 53' 22.15"	7	Terrestrial moss frag.	-23.7	1980 ± 30	1930–1830	68.3	2000–1750	95.4	1890	1890 ± 100	Moss in till, overlying 6-7 m amsl raised beach
14	ART-07A-2015	ETH-69688	62° 10' 51.73"	58° 51' 39.45"	18	*Laternula* sp.shell	-0.9	7045 ± 85	6790–6480	68.3	6940–6330	95.4	6630	6640 ± 300	Shell in fine sediments; max. glacial readvance age
15	ART-07B-2015	ETH-69689	62° 10' 51.73"	58° 51' 39.45"	18	*Laternula* sp.shell	4.0	6590 ± 70	6270–6000	68.3	6400–5880	95.4	6140	6140 ± 260	Shell in fine sediments; max. glacial readvance age
16	ART-07C-2015	ETH-69690	62° 10' 51.73"	58° 51' 39.45"	18	*Laternula* sp.shell	0.0	6730 ± 75	6440–6160	68.3	6570–6000	95.4	6300	6290 ± 280	Shell in fine sediments; max. glacial readvance age
17	ART-09A-2015	ETH-69691	62° 10' 50.59"	58° 51' 40.66"	27	*Laternula* sp.shell	-2.2	6265 ± 75	5920–5640	68.3	6090–5530	95.4	5790	5790 ± 280	Shell in till; max. glacial readvance age
18	ART-09B-2015	ETH-69692	62° 10' 50.59"	58° 51' 40.66"	27	*Laternula* sp.shell	3.4	5895 ± 70	5550–5280	68.3	5660–5080	95.4	5400	5390 ± 280	Shell in till; max. glacial readvance age
19	ART-10A-2015	ETH-69693	62° 10' 49.04"	58° 51' 34.88"	28	*Laternula* sp.shell	0.9	6235 ± 70	5890–5620	68.3	6020–5480	95.4	5760	5760 ± 260	Shell in till; max. glacial readvance age
20	ART-10B-2015	ETH-69694	62° 10' 49.04"	58° 51' 34.88"	28	*Laternula* sp.shell	-1.2	5925 ± 70	5560–5300	68.3	5700–5130	95.4	5430	5420 ± 260	Shell in till; max. glacial readvance age
21	ART-10C-2015	ETH-69695	62° 10' 49.04"	58° 51' 34.88"	28	*Laternula* sp.shell	-2.8	6520 ± 75	6200–5930	68.3	6330–5780	95.4	6070	6070 ± 260	Shell in till; max. glacial readvance age
22	ART-04A-2015	ETH-69684	62° 10' 23.69"	58° 54' 59.09"	42	*Laternula* sp.shell	-1.4	>44300 ± 4430	45510–45040	68.3	45730–44830	95.4	45280	45280 ± 460	Shell in fine silty/sand thrust-up marine sediments
23	ART-04B-2015	ETH-69685	62° 10' 23.69"	58° 54' 59.09"	42	*Laternula* sp.shell	2.8	>43700 ± 4370	44970–44580	68.3	45210–44430	95.4	44790	44800 ± 400	Shell in fine silty/sand thrust-up marine sediments
24	ART-05A-2015	ETH-69686	62° 10' 24.55"	58° 54' 59.05"	42	*Laternula* sp.shell	2.8	>48500 ± 4850	50090–49170	68.3	50800–48710	95.4	49690	49720 ± 1120	Shell in fine silty/sand thrust-up marine sediments
25	ART-05B-2015	ETH-69687	62° 10' 24.55"	58° 54' 59.05"	42	*Laternula* sp.shell	-	>51700 ± 5170	51900–51490	68.3	52120–51300	95.4	51700	51700 ± 400	Shell in fine silty/sand thrust-up marine sediments
26	K1-M [0–0.5 cm]	Beta-501582	62° 11' 36.55"	58° 57' 59.93"	15	*Drepanocladus l.* sp. AM	-27.4	-100 ± 30	-6 – -7	68.3	-5 – -7	95.4	-6	-6 ± 1	Aquatic moss living in lake; collected 2011 CE
27	K2-M [4.5-5 cm]	Beta-516809	62° 11' 36.55"	58° 57' 59.93"	15	*Drepanocladus l.* sp. AM	-29.3	-130 ± 30	-6 – -7	68.3	-6 – -7	95.4	-7	-7 ± 1	Aquatic moss living in lake; collected 2011 CE
28	K3-BS [5-6 cm]*	Beta-516810	62° 11' 36.55"	58° 57' 59.93"	15	Bulk lake sediment	-18.4	1350 ± 30*	650–460	68.3	750–370	95.4	560	560 ± 180	Orange-brown silt; old carbon LRE= 700±100 yrs
29	K4-BS [9–10 cm]*	Beta-504801	62° 11' 36.55"	58° 57' 59.93"	15	Bulk lake sediment	-23.9	1600 ± 30*	910–700	68.3	1010–600	95.4	800	800 ± 200	Orange-brown silt; old carbon LRE= 700±100 yrs
30	K5-BS [20–21 cm]*	Beta-497408	62° 11' 36.55"	58° 57' 59.93"	15	Bulk lake sediment	-32.6	9380 ± 30*	10030–9790	68.3	10130–9660	95.4	9910	9900 ± 240	Grey silt-clay; old carbon >>LRE= 700±100 yrs
31	K6-BS [36.5–37 cm]	Beta-501584	62° 11' 36.55"	58° 57' 59.93"	15	Bulk lake sediment	-18.0	1860 ± 30	1820–1770 / 1750–1700	27.8 / 40.5	1830–1690 / 1650–1620	90.6 / 4.9	1750	1750 ± 100	Orange-brown silt; Low carbon AMS micro-sample
32	K7-BS [45.5–46 cm]	Beta-501585	62° 11' 36.55"	58° 57' 59.93"	15	Bulk lake sediment	-17.7	3350 ± 30	3570–3480 / –	68.3 / –	3680–3670 / 3640–3450	1.0 / 94.5	3530	3530 ± 100	Orange-brown silt; Low carbon AMS micro-sample
33	K8-BS [73.5–74.5 cm]	Beta-498331	62° 11' 36.55"	58° 57' 59.93"	15	Bulk lake sediment	-18.0	6410 ± 30	7420–7390 / 7330–7250	9.1 / 29.2	7430–7240 / 7210–7170	85.5 / 10.0	7300	7300 ± 120	Bulk orange-brown silt; δ^{13}C value=terrestrial

Table 2. New radiocarbon age data from the eastern Shetland I Moraine and the Kiteschsee Lake record on Fildes Peninsula. Calibrated ages have been rounded to the nearest 10 years. Dating replicates were used to assess dating and interpretation accuracy. Elevation data (Alt. m a.s.l. – Altitude in metres above present sea level) were taken with a Garmin handheld GPS map 62stc, precision ±2 m (latitude, longitude) and altitudinal precision of ±5–10 m.
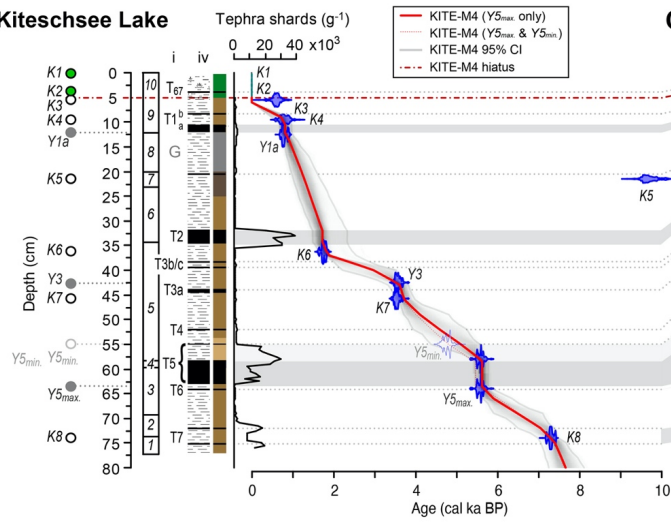
Kiteschsee Lake record

The new Kiteschsee Lake record shown in Figure 4A, B provides a continuous and well-defined mid–late Holocene record of palaeoenvironmental change and volcanic eruptions, most likely from nearby Deception Island, and is largely devoid of substantial post-eruption and soliflucted ash and catchment reworking, which commonly disrupt other lake sediment records from King George Island, e.g., Yanou Lake - Figure 4C, Ardley Lake, Belen Lake, Long Lake (Watcham et al., 2011; Roberts et al., 2017).

Lithology and geochemistry: High-resolution (0.5 cm interval) sedimentological, XRF core scanning (XRF-CS) geochemical analysis (200 μm contiguous scanning) and tephra glass-shard counting revealed several prominent visible volcanic ash (tephra) layers, some of which define the boundaries of the ten Lithofacies Units (henceforth, Units), described below (Figure 4). Coherent downcore changes in Ti, K, Ca indicated geochemical changes were primarily driven by catchment erosion of (volcanic) bedrock and overprinted by airfall and reworked tephra deposits (Figure S2, S3, S4). Downcore peaks in Ln(Ca/Ti) and sand content largely mirror the incoherence/coherence scatter ratio profile (inc./coh.; organic content proxy) and were used to define the precise positions of the visible tephra layers (Figure 4A–B S2, S3). Shard-specific major-element geochemistry from the two most prominent tephra layers at 33 cm (mean; 95% range: 1,730; 2,420–1,470 a cal BP) (labelled T2 in Figure 4A–B) and 59 cm (5,600; 5,740–5,450 a cal BP) (T5 in Figure 4A–B) have a similar airfall thickness to the airfall components of the two most prominent mid–late Holocene tephra deposits in nearby Fildes Peninsula lake records (Watcham et al., 2011; Roberts et al., 2017).
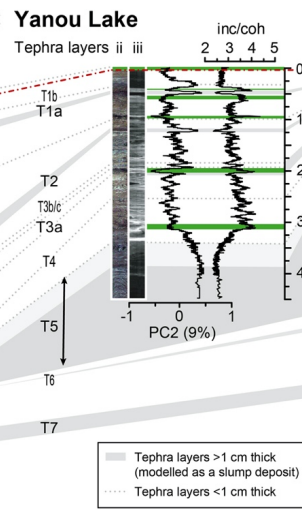
23
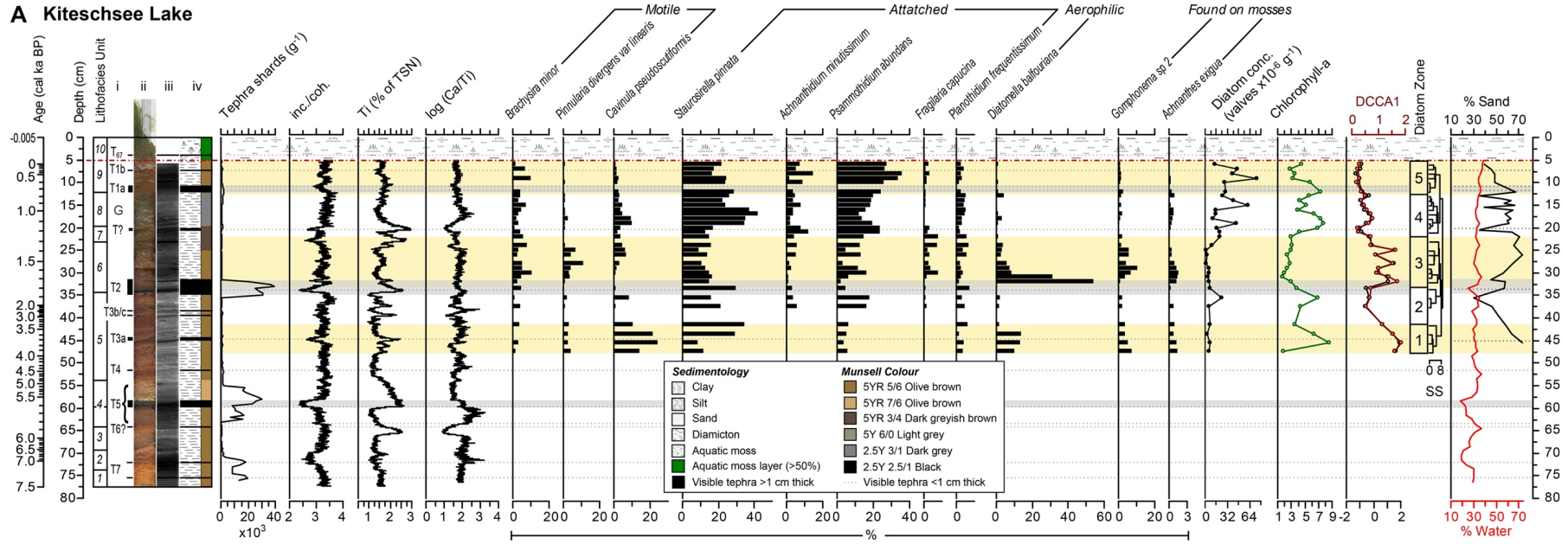
A Kiteschsee Lake

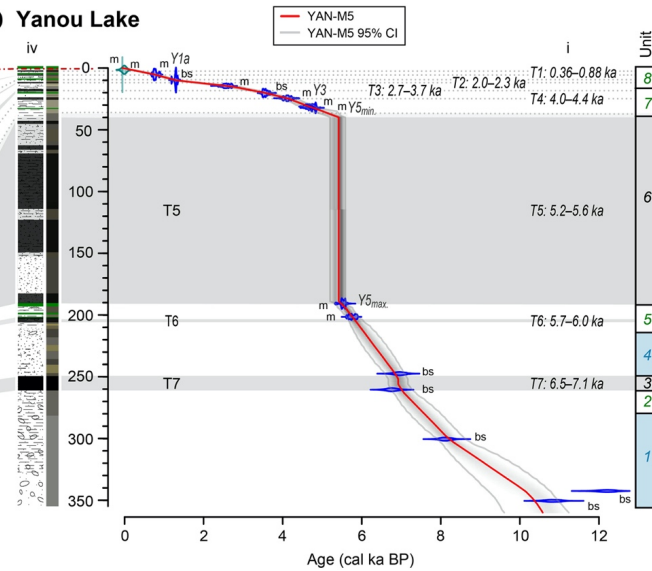**B** Kiteschsee Lake

C Yanou Lake

D Yanou Lake

Figure 4. Summary of key stratigraphic, diatom and chronological data from the Kiteschsee Lake record. Lithofacies units are as defined by cluster analysis of XRF-CS data. I = Tephra layers in the Kiteschsee Lake record, II = ITRAX-XRF optical image, III = ITRAX X-radiograph (positive image), IV = Summary lithology and RGB Munsell colour. B) Bayesian age-depth model for the Kiteschsee Lake record K1–8 are radiocarbon ages shown in Table 2, T1a, T3a, T5 and T7 are correlation ages of tephras in the Yanou Lake record (see Table S2). C–D) Tephrastratigraphic correlation with the Yanou Lake record and the updated Bayesian age-depth model (2020 calibration) for the Yanou Lake record.

Both contained rhyolitic glass shards whose geochemistry was more similar to tephra layers previously linked to mid Holocene eruptions from the Deception Island volcano than tephra deposits from South America (Supplementary Materials details).

Chronology: Eight radiocarbon ages from the 77 cm long, c. 7,600-year-old sediment core record from Kiteschsee Lake were broadly in chronological order, except for a calibrated age of 9,900±240 a cal BP near the base of the fine grey (glaciofluvial) silt and clay deposits of Unit 8 at 21–22 cm depth (Table 2). Bulk sediments at 7–8 cm, 54.5–55 cm, 64.5–65 cm depth could not be dated due to insufficient carbon. The age depth model for the new Kiteschsee Lake record, shown in Figure 4B and described in Supplementary Note 2, had the best fit to calibrated and reservoir-corrected radiocarbon age data (Figure 4C–D; Table 2). To summarise, the Kiteschsee Lake record has a basal age of 7,470 a cal BP at 77 cm depth (weighted mean modelled age) (7,820–7,110 cal a BP min.–max. 95% confidence age range; 7,480 cal a BP median age). The mean 95% confidence age range is 470 years, with a minimum 95% confidence age range of 4 years at 4.5 cm, in the post-bomb era and a maximum 95% confidence age range of 1,230 years at 51.5 cm; 83% of the measured ages overlap with the age-depth model (95% ranges).

Lithofacies Units: Basal lithofacies Units 1–3, 77–60 cm (7.5–5.6 ka cal BP, mean modelled ages) are composed of poorly sorted olive-brown silt with three prominent fine black ash layers in Unit 2 (Figure 4, S2–8; Supplementary Note 2). Following the initial deposition of the T5

25

tephra (Unit 4: 60–58 cm; 5.6–5.5 ka cal BP), there is a distinct change to a light orange-brown silty-clay close to the base of Unit 5 (Figure 4; S2). The similar geochemistry of Unit 6 and the light grey clayey mud of Unit 8 suggests a glacial transgression could have begun as early as 1.7 ka cal BP (the basal age of Unit 6, at 34 cm). After a return to olive-brown silt in Unit 7 (similar to Unit 5) the most prominent visible change in lithology in the record (tephra layers aside) occurs at c. 20 cm depth (c. 1.2 ka cal BP), with the deposition of a light grey clayey-mud lithofacies unit containing sand-rich layers (Unit 8: 20–12 cm depth; 1.2–0.5 ka cal BP).

Elevated dry mass accumulation rates and increased sand deposition within Unit 6 and the glaciogenic Unit 8 are indicative of increased erosion and meltwater input from c. 1.7 ka cal BP onwards (Figure S3, S8). Notably, radiocarbon age of 9,380±30 ^{14}C years from 21–22 cm depth at the base of Unit 8 had a heavily depleted δ^{13}C value of −32.6 ppm, likely due to glacial reworking of old (possibly marine) carbon deposited in/around the Davies Heights massif during early Holocene deglaciation (Table 1). Unit 9 (12–5 cm; 0.78– -0.005 ka cal BP) is composed of laminated olive-brown silt, similar to Units 5 and 7. Its uppermost sediments, immediately below the living aquatic moss, have a measured radiocarbon age of 1,350±30 ^{14}C years (1.2±0.8 ka cal BP) implying bulk sediment radiocarbon ages obtained from Unit 9 are either significantly less influenced by old carbon, sedimentation rates declined significantly or some sediment is missing between Units 9 and 10. While a hiatus could have existed in the transition between the sedimentary lake environment and the sub-aquatic moss environment at 5 cm (Unit 10), it appears that the missing sediment was incorporated into the overlying aquatic moss layer when it established its root structure (Figure S1).

Diatom analysis: Overall, diatom analysis revealed ontogeny within the Kiteschsee Lake record is characterised by shorter term changes in diatom communities superimposed upon the steady ecological and environmental evolution of the lake during the Holocene. Redundancy

analysis (RDA), using key geochemical variables associated with tephra obtained by XRF-CS analysis, showed that tephra deposition did not have a significant impact on the diatom community composition in the Kiteschsee Lake record (p=0.596) (Figure S9, S10). While certain species found in the record respond directly to climatic variables (i.e., wind speed, temperature and precipitation), the overall community structure response in Kiteschsee Lake was primarily associated with changes lake-ice cover and turbidity, which are indirectly related to temperature change and ice expansion. Deglaciation and warming can have a significant impact on catchment processes affecting nutrient supply to lakes and diatom compositional turnover (β-diversity, DCCA score) and turbidity within lakes, which is driven by increased (glacial) erosion and/or increased wind strength when lakes are seasonally ice-free.

Variations in key indicator species and the reconstructed chlorophyll-a were used to examine the impact of climate-driven glacier readvances in the mid-southern BIC foreland (Figure 4, 5). A notable shift in μ-XRF geochemistry exists at c. 60 cm depth (Figure S1), but we found no clear bio-geochemical evidence of (glacio) marine sedimentation. Although diatom concentration in the lowermost zone was too low for quantitative analysis, all sedimentary units younger than c. 6 ka cal BP (c. 63 cm) contained freshwater diatoms. The $\delta^{13}C$ value from 73.5–74.5 cm depth is also consistent with a freshwater sedimentary environment, implying that it is younger than c. 6.5 ka cal BP. Using constrained cluster analysis (Figure 4A, S9), we divided the diatom record from 47 cm upwards into five zones described in detail in Supplementary Note 2. The increase in diatom accumulation rate from c. 1.9 ka cal BP is linked to the increased input of glaciogenic sediments and dry mass accumulation rate between c. 1.9 and 1.6 ka cal BP (Figure S8). The transition to increased meltwater input in lithofacies Unit 8 coincides broadly with the start of Diatom Zone 4 (22–13 cm: 1.3–0.8 ka cal BP). Diatom Zones 4 and 5 are of most interest in this paper because they correspond to the decline in

aerophilic and littoral diatom species and concurrent increases in species associated with more turbid conditions (e.g., *Stauriserella pinnata*), and lower DCCA scores (Figure 5F, S9).

The trends initiated in Diatom Zone 4 continued in Zone 5 until ~5 cm depth (mid-late C20th onwards), when there was a significant shift to an aquatic moss (*Drepanocladus longifolius* (Mitt. Paris) sp.) dominated environment. The low DCCA Axis 1 (β-diversity) values in Zone 5 reflect a more-persistently turbid lake environment, indicating (strong) wind and/or glacially driven reworking and resuspension of sediment in the lake (Figure 5B). This occurred at the same time as persistently lower reconstructed summer air temperatures in the nearby Yanou Lake record (Figure 5G, S11) (Roberts et al., 2017). The most significant changepoint in the Yanou Lake reconstructed temperature record at 1.3 ka cal BP (Figure S11) marks a shift to colder temperatures and a return to more turbid conditions in Kiteschsee Lake (Figure 5B, C).

Discussion

In this section, we use new and published cosmogenic and radiocarbon ages, and lake sediment data, to assess the deglaciation and glacial readvance history of the BIC in the mid–late Holocene. We have divided the discussion into four readvance stages, grouping the eight probability 'gaps' that represent possible readvances on Fildes Peninsula and King George Island as follows: Stage 1: c. 7 ka readvance/standstill (7.4–6.6 ka cal BP); Stage 2: mid Holocene retreat followed by minor readvances (to and within the Shetland I moraine present day limits) at 5.3–4.8 ka cal BP; 4.5–3.9 ka cal BP; 3.3–3.0 ka cal BP; 2.6–2.2 ka cal BP; Stage 3 readvance: 1.7–1.3 ka; Stage 4 readvances: 1.3–0.7 and <0.7 ka cal BP. We assess the main mechanisms for Holocene climate change on the Antarctic Peninsula identified in Bentley et al. (2009) (principally, solar insolation, SWW, SAM) and other potential drivers (e.g., volcanism; Cole-Dai et al., 2021; Mann et al., 2021) of centennial to millennial-centennial scale climate change and glacier variability on King George Island.
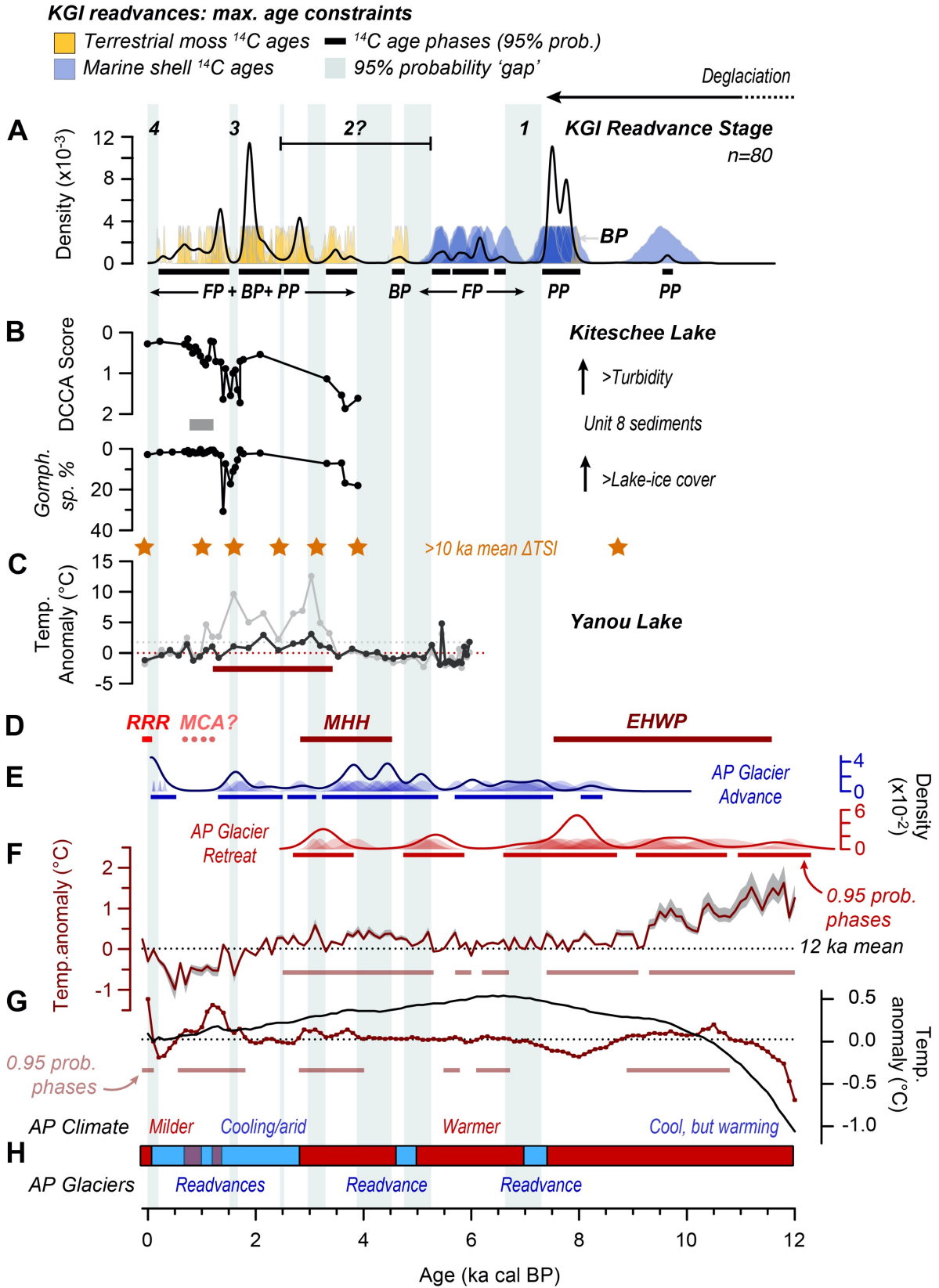
28

Figure 5. Regional palaeoclimatic context for Holocene glacier fluctuations on the South Shetland Islands, Antarctic Peninsula. A) Probability density phase model for maximum age constraints on glacier readvances on King George Island between 12–0 ka cal BP (Figure 3D for details). The timing of the King George Island (KGI) Readvance Stages 1–4 is shown. Light

grey vertical shaded zones represent 95% probability 'gaps' when readvances could have occurred; BP=Barton Peninsula; FP=Fildes Peninsula, PP=Potter Peninsula. B) Diatom-inferred reconstructions and key indicator diatom species for Kiteschsee Lake. Lower DCCA scores reflect more turbid conditions, and lower *Gomphonema* sp. percentages represent less aerophilic conditions, and longer seasonal ice-cover. C) Glycerol dialkyl glycerol tetraether (GDGT)–mean summer air temperature (MSAT) anomaly reconstruction (light grey) from Yanou Lake (Foster et al., 2016; Roberts et al., 2017) (RMSE = 2.45 °C, not shown for clarity); the dashed line is the 6 ka mean MSAT anomaly for the dataset published in Roberts et al. (2017); the black line and datapoints represent a revised (interim) MSAT anomaly reconstruction for Yanou Lake (see Supplementary Materials for details). This and 6 kyr mean±1σ $MSAT_{anomaly}$ of 0.06±1.50 °C are more realistic than the previously published MSAT-GGDT data; orange stars are ΔTSI peaks (see Figure 7). D) Climate syntheses for the Antarctic Peninsula (Ingólfsson et al., 2003; Bentley et al., 2009). E) Probability density phase model for glacier advance (blue) and retreat (red) data on the northern Antarctic Peninsula in Kaplan et al. (2020). F) Temperature anomaly data from the James Ross Island (JRI) ice core record, NE Antarctic Peninsula (Mulvaney et al., 2012); grey shading is the as published ±error. G) Holocene palaeotemperature compilation showing the median temperature anomaly for 60–90 °S stack (dark red line) and the global temperature stack anomaly (black line) (Kaufman et al., 2020). The grey dashed line is the average median 12-kyr value for 60–90 °S temperature proxy data (0.02); errors in both datasets are mostly out of range and not plotted for clarity.

Early to mid Holocene deglaciation

Previously published lake sediment records show that the terrestrial deglaciation of the southern-mid part of Fildes Peninsula from LGM limits dates to c. 12–9 ka cal BP (Mäusbacher et al., 1989; Watcham et al., 2011) (Figure 1), and was broadly coeval with other areas of the SSI (Palacios et al., 2020). New radiocarbon data from the BIC foreland and Potter Cove show the ice cap had thinned and retreated substantially during the early Holocene, with large parts of the Fildes Peninsula and Potter Peninsula becoming ice free by c. 8 ka cal BP. The BIC had also retreated from the central Fildes Peninsula area by c. 8 ka (Figure 1, 6A, 7E). New chronological evidence from the BIC foreland and the Shetland I moraine in this study is consistent with the deglaciation of Mondsee Lake (Figure 2), 45 m a.s.l., ~1,500 m away from the present glacier margin at this time (Schmidt et al., 1990). Recession progressed towards the higher elevation areas in the eastern sector located, above the C20th ELA of ~150 m a.s.l., into areas located in depressions next to the former ice limit, and triggered an increased rate of isostatic uplift and falling relative sea level (Figure 7E, F) (Watcham et al., 2011).
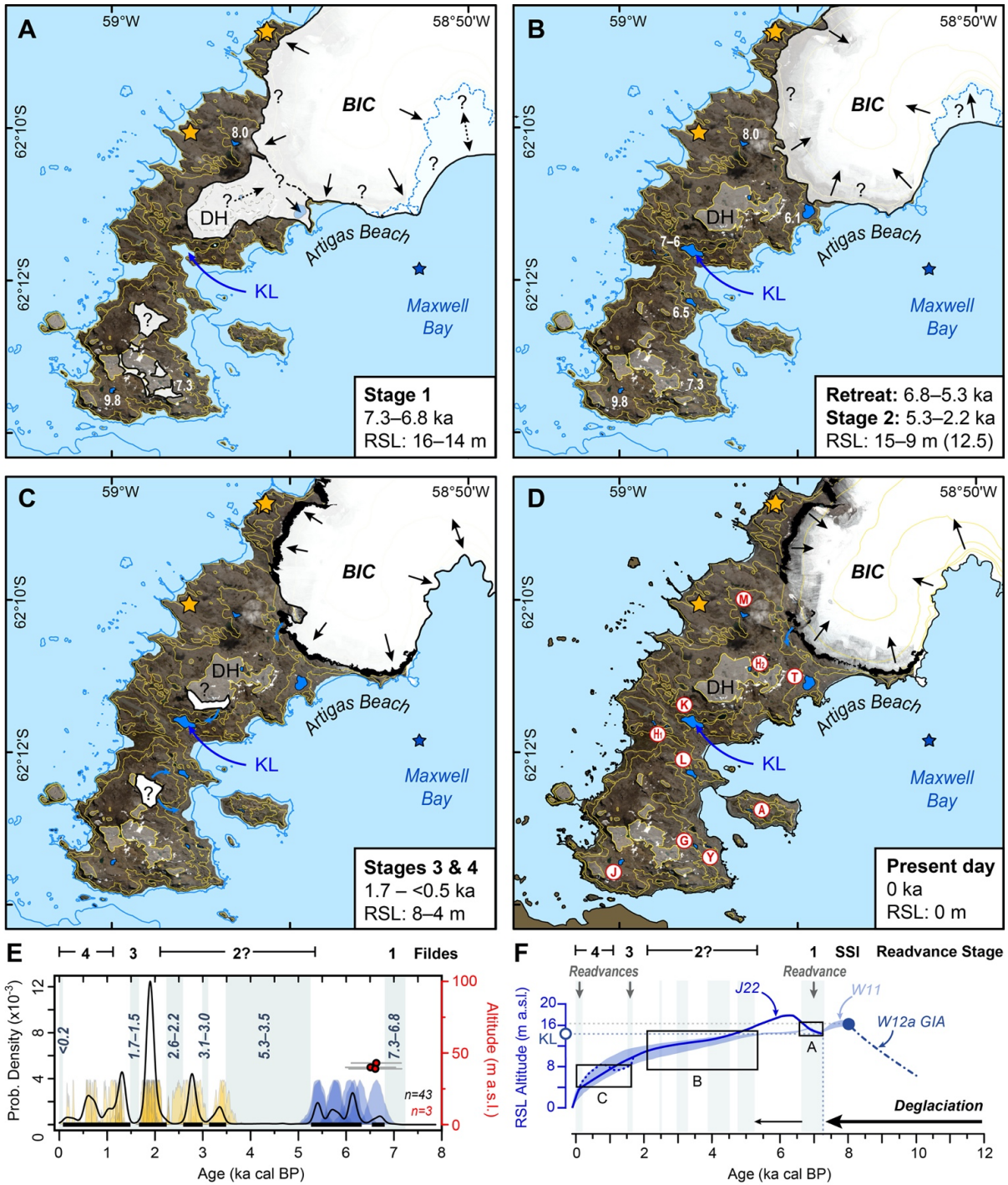
Figure 6. A–D) Schematic reconstruction of mid–late Holocene glacier readvance extents during Stages 1–4 on Fildes Peninsula. Glacier extents shown in A–C are based on a compilation of new and published chronological data (panel E) for the Shetland I moraine (dark shading in C and D). E) Radiocarbon ages and probability density phase model for age constraints on glacier readvance on Fildes Peninsula (n=43; see Figure 3C for details; yellow distributions are radiocarbon ages of terrestrial material embedded in moraines; blue distributions are radiocarbon ages of marine material embedded in moraines; red circles with grey external error bars are ^{10}Be cosmogenic nuclide exposure ages obtained from boulders (orange stars in A–D). F) Summarised relative sea level (RSL) curves for the South Shetland Islands (Watcham et al., 2011 – W11; Whitehouse et al., 2012a, b – W12aGIA; Johnson et al., 2022 – J22) used to determine the elevation of the coastlines in panels A–C; BIC = Bellingshausen Ice Cap; DH = Davies Heights; KL = Kiteschee Lake, which is a marine

embayment in A; the blue star is the location of Maxwell Bay marine records referred to in the text (Milliken et al., 2009; Simms et al., 2011); white areas (90% transparency) bordered by solid black lines in A–C are schematic representations of BIC extent on the Fildes Peninsula for each stage; present-day moraines mapped in this study are shown in D; black arrows represent schematic glacier flow directions, except in B where they represent retreat close to (or within) present day limits between 6.8–5.3 ka BP, followed by minor readvances close to present limits between 5.3–2.2 ka BP; blue arrows are main meltwater pathways. Question marks in A and B indicate uncertain locations of the glacier fronts with lakes sediment basal and/or freshwater transition ages shown as white text (in ka BP; as Figure 1). Black shaded areas around the BIC in C and D are the last readvance moraines (as Figure 2). The 2013 CE satellite image of the BIC is shown in D, along with studied lakes in blue (labelled as Figure 1: white circles/red borders). Yellow lines are contours at 20 m, 40 m and 100 m elevation, with areas >100 m shaded white (30% transparency). The VHR satellite image in A–D is from Maxar Products: WorldView-2 image acquired 11th April 2013 © 2021 Maxar Technologies. This figure includes material copyright of Maxar Technologies, All Rights Reserved, reproduced here at low resolution with permission under a NERC-BAS educational license and not included as part of a Creative Commons license.

Stage 1 readvance (c. 7 ka)

Evidence of the Stage 1 readvance and a marine transgression, when relative sea-level was ~15 m a.s.l. after 7.5–7.0 ka cal BP in Potter Cove (Strelin et al., 2014) is consistent with radiocarbon ages from Potter Peninsula constraining deglaciation and cosmogenic evidence from Fildes Peninsula constraining retreat after a readvance of the BIC across NW foreland at c. 7 ka cal BP (Figure 3, 5A, 6A, 7E-G). Watcham et al. (2011) established an upper Holocene marine limit of ~16 m a.s.l. at c. 8.0 ka cal BP, with a short-lived fall and return to that level at 7.0 ka cal BP indicative of a standstill in glacier retreat or a minor readvance.

Data constraining RSL from the SSI are more complex than other locations across Antarctica, and several different RSL curves have been suggested for the SSI (Pallàs et al., 1997; Bentley et al., 2005; Hall, 2010; Roberts et al., 2011; Watcham et al., 2011; Simms et al., 2012; 2021; Johnson et al., 2021). Bentley et al. (2005) initially proposed that RSL declined from an undated early-mid Holocene marine limit of ~16–18 m above present sea-level (henceforth, m a.s.l.) in a discontinuous manner, interrupted at 14.5-16 m a.s.l. by a redavance between 5.8–3.0 ka cal BP). In contrast, and with more data, Hall (2010) and Watcham et al. (2011) both suggested RSL fall was largely continuous after 6 ka cal BP. A readvance at c. 7 ka is consistent

with evidence of marine-freshwater transitions in isolation basins between 14–16 m a.s.l. on the Fildes Peninsula (cf. Watcham et al., 2011).
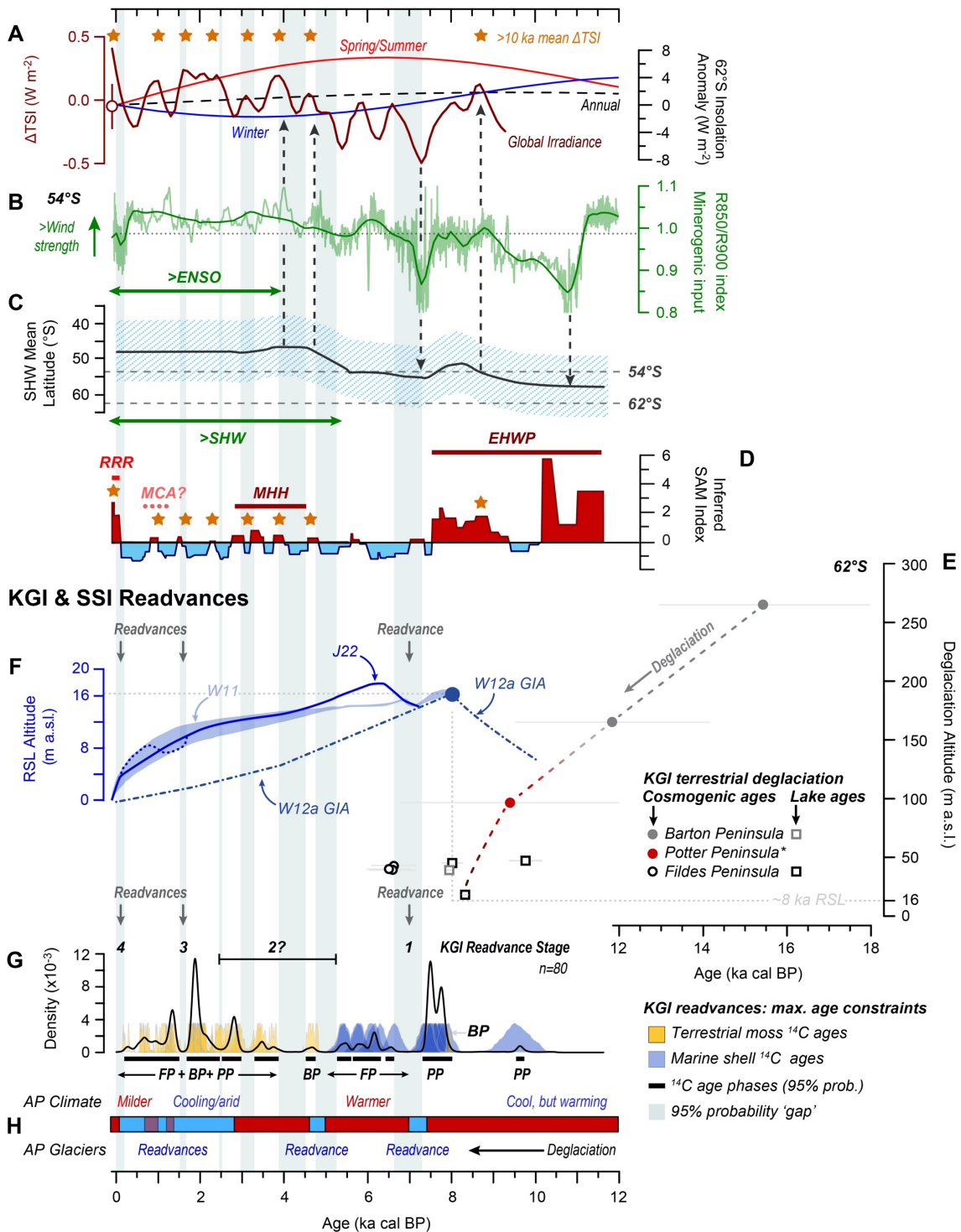

Figure 7 Mechanisms of deglaciation and glacier fluctuations on Potter Peninsula. A) Total Solar Irradiance, as ΔTSI, which represents the deviation from present day value (Steinhilber et al., 2009), compared with annual (dotted black line), austral spring/summer (SONDJF) (red line), and winter (JJA) (blue line) solar insolation received at 62°S during the Holocene (11.75

ka) (Laskar et al., 2004). The open red circle is the mean±1σ ΔTSI value for the last 10 ka; orange stars mark ΔTSI peaks greater than the 10 ka mean value. B) Ultra-high resolution (69 µm) hyperspectral (SPECIM) R850/R900 data, a proxy for mineral input into the Emerald Lake, Macquarie Island at 54°S (Saunders et al., 2018), which reflects changes Southern Hemisphere Westerly wind (SHW) strength during the mid–late Holocene; the dark grey horizontal dotted line is the R850/R900 dataset mean; dark green line is 100-year interval LOESS smoothing of the R850/R900. C) Hypothetical representation of changes in the mean annual latitudinal position of the core SHW intensity belt (dark grey line) and approximate 1σ latitudinal range of enhanced precipitation (light blue stipple) (Ariztegui et al., 2010; Quade and Kaplan, 2017). In reality, the SHW are more intense and focused during positive (warmer) phases of the SAM, but weaker, latitudinally broader and less focused during negative (colder) phases of the SAM, show in D. The light grey horizontal dashes are 54°S (Macquarie Island) and 62°S (South Shetland Islands); vertical dashed lines and arrows highlight the key hypothesised latitudinal shifts of the Holocene and their relationship to the global irradiance profile shown in A; ENSO = El Niño Southern Oscillation. D) Inferred Holocene SAM-index variability between positive (red) to negative (blue) SAM-like states based on Northern Arboreal Pollen data from Southern Chile (Moreno et al., 2018; Reynhout et al., 2019) (sub-figure adapted from Kaplan et al. (2020) with permission, Kaplan pers. comm.); EHWP = Early Holocene Warm Period; MHH = Mid Holocene Hypsithermal; MCA = Medieval Climate Anomaly; RRR = Recent Rapid Regional warming, from Bentley et al. (2009). E) Summarised relative sea level (RSL) envelope for the SSI (W11; light blue shading; Watcham et al., 2011) compared with the RSL curve in Johnson et al. (2022) (J22; dark solid and dotted blue lines) and the W12a GIA model (Whitehouse et al., 2012a, b); see original references for further details and data. F) Cosmogenic nuclide exposure ages and key lake basal age constraints on deglaciation for terrestrial ice-free peninsulas on KGI at different altitudes from Barton Peninsula (Seong et al., 2008), Potter Peninsula (this study) and Fildes Peninsula (Heredia Barión et al., submitted) (secondary plot); * = new data (this study).

Following the readvance at c. 7 ka cal BP, new cosmogenic exposure ages from erratics in this study show the NW marine platform close to the present ice-front on Fildes Peninsula was ice-free by 6,580±440 years ago (Figure 7E, Table 1). We found no evidence for cosmogenic nuclide inheritance, therefore, these erratics had not been reworked or eroded from pre-Pleistocene formations on the SSI and were most likely glacially-transported from the Antarctic Peninsula prior to (or during) the LGM, then fully reset by reworking immediately prior to deglaciation. Tiefersee Lake and Hochlandsee Lake, located ~800 and ~1500 m from the present-day ice cap, also became ice free (Figure 2, 3E) (Mäusbacher et al., 1989; Mäusbacher, 1991).

Marine sediments with bivalve shells dated to between 6.8 and 5.3 ka cal BP (95% probability phase range; Figure 5A), were reworked into till at the extreme east of the Shetland I moraines,

during a subsequent readvance, most likely between 5.3–3.9 ka cal BP as RSL fell below 15 m a.s.l. (Figure 2, 6B, 7E; Table 2, S3). Moraines in this area were located close to the former sea-level prior to reworking, and Holocene raised beaches up to c. 16–18 m a.s.l. extended under the BIC in the Artigas Beach area may have survived relatively unmodified beneath the ice cap (John and Sugden, 1971; Hall, 2003).

Persistently warmer atmospheric temperatures across the Peninsula between 7 and 6 ka cal BP led to reduced sea-ice and warmer-than-Holocene-average sea-surface temperatures in marine sediment records from Maxwell Bay and the Palmer Deep between 8.2 and 5.9 ka cal BP (Milliken et al., 2009; Mulvaney et al., 2012; Etourneau et al., 2013). Overall, the marine-terminating BIC was less extensive during this shell colonization phase between 6.8–5.3 ka cal BP (Hall, 2007; Fretwell et al., 2010), and had retreated within its present-day limits by c. 6.0 ka cal BP, with a glacier front (re)occupying the inner bays of Collins Harbour in Maxwell Bay (Mäusbacher et al., 1989; Tatur et al., 1999; Yoon et al., 2006; Milliken et al., 2009; Simms et al., 2011; Watcham et al., 2011; Chu et al., 2017). Elsewhere on the Peninsula and around Antarctica ice sheets thinned and ice shelves retreated (Roberts et al., 2008; Hein et al., 2016; Verleyen et al., 2017; Johnson et al., 2020). Windier conditions at this time in the Southern Ocean have been linked to rising global temperatures in the early to mid Holocene (Marcott et al., 2013; Saunders et al., 2018; Kaufman et al., 2020) (Figure 5G, 7B, 7C).

Stage 2 Readvances

Evidence for extensive glacier readvances on KGI and SSI is limited in the mid-late Holocene. Between c. 6.0 and 2.8 ka cal BP, warmer-than-Holocene-average atmospheric temperatures across the Antarctic Peninsula (Figure 5F) led to extensive moss banks and the formation of widespread lacustrine moss deposits on KGI (Figure 3E) (Björck, 1991a; Björck, 1991b; Sun et al., 2005; Hall, 2007; Bentley et al., 2009; Mulvaney et al., 2012; Foster et al., 2016; Roberts

et al., 2017). Aquatic moss was continuously present between 6.0–4.5 ka cal BP (Figure 3E) (Milliken et al., 2009; Watcham et al., 2011; Roberts et al., 2017).

We found no direct evidence of BIC readvance on the Fildes Peninsula beyond its present-day limits between 5.3–3.9 ka cal BP, but it seems likely that the general warming transition into the mid Holocene Hypsithermal (MHH) (as defined by Bentley et al. (2009)) was interspersed by at least one minor/short-lived readvance (Figure 3D, 5E, 5H). A Stage 2 readvance ^{14}C data probability 'gap' between 5.3–4.8 ka cal BP (Figure 5A) overlaps with a hypothesised local readvance in the Stranger Point area of Potter Peninsula at c. 5 ka cal BP (Emslie et al., 2019), with persistently colder temperatures in the Yanou Lake record between 6.0–3.7 ka cal BP, and glacier readvances elsewhere on the NAP (Figure 5C, E, H). Surface temperatures decreased, and sea-ice cover increased in Maxwell Bay between c. 5.9 and 2.6 ka cal BP and summer sea-ice occupied the inner Collins Harbour of Maxwell Bay until at least c. 1.7 ka cal BP (Simms et al., 2011).

Stage 3 readvance (late Holocene Neoglacial)

Most of the present-day Shetland I moraine was established during Stage 3 and/or Stage 4 readvances. New mean radiocarbon ages between c. 2.0 and 1.2 ka cal BP from moss fragments incorporated into a small moraine on top of a raised beach at 7–6 m a.s.l. on Artigas Beach, indicate that glacial readvance during the late Holocene in this sector of the BIC was restricted, and probably occurred in two stages: first, after the formation of the raised beach and sometime between c. 1.7 and 1.4 ka cal BP (Stage 3 readvance) and at <0.7 ka cal BP (Stage 4 readvance).

The former occurred shortly after the start of the 'Neoglacial' on the Antarctic Peninsula (Bentley et al., 2009). New radiocarbon ages constrain the initial formation of the present-day Shetland I moraine from Valle Norte towards its eastern extension (see Figure 2 for location),

where moraines are still ice-cored and in contact with the ice. We found moraine crests several meters above the ice-level, similar to those found in Valle Norte (Hall, 2007), which post-date c. 1.2 ka cal BP, the age of the youngest new sample dated. This age means that the eastern part of the BIC was landward of its present limit, with mosses colonizing its foreland until at least 1.2 ka cal BP.

Data imply that the BIC only readvanced by tens of metres relative to its present position in the Artigas Beach area in the second half of the late Holocene. Hall (2007) determined that glacier readvance of the Shetland I moraines occurred at Valle Norte and Valle Klotz (Figure 1 for locations) between c. 1.0 and 0.7 ka cal BP (Figure 2, 3C, 5A). The ice in these areas advanced in lobes, which spread out into ice-marginal depressions, forming several small thrust moraines, c. 300 m from the prominent moraine ridges (dated in this study).

The Stage 3 readvance was broadly synchronous with two minor phases of glacier expansion on the north-eastern AP (Kaplan et al., 2020) (Figure 5E), in Southern South America between c. 1.5 and 1.1. ka cal BP (Strelin et al., 2014; Moreno et al., 2018), and a predominantly warmer phase in composite ice core records from elsewhere in Antarctica (Masson et al., 2000).

Stage 4 readvances and the 'last readvance'

Stage 4 probability 'gaps' in the Shetland I moraine radiocarbon ages (Figure 3) imply readvances could have occurred at c. 0.7, 0.4 and/or <0.2 ka cal BP. These ages broadly coincide with more sustained colder conditions in the Yanou Lake palaeotemperature record from the outermost Fildes Peninsula (Roberts et al., 2017), and increased lake-ice cover, greater turbidity and reduced productivity in Kiteschsee Lake (Figure S5F, S11). Although currently ice-free, the Davies Heights is located close to the present-day ELA and could have sustained more permanent ice-cover even with a relatively minor reduction in temperature (Figure 6C).

The Stage 4 readvance followed the Medieval Climate Anomaly (MCA) (c. 1.2 and 0.8 ka cal BP - Bentley et al. (2009); c. 1400–800 CE – Lamb (1965); 1250–950 CE - Mann et al. (2009). Increased fine-grained sedimentation in from Potter Cove during the MCA and has been linked to warmer conditions, including warmer sea surface temperatures from the western Antarctic Peninsula (Milliken et al., 2009; Hass et al., 2010; Watcham et al., 2011; Etourneau et al., 2013). Some Southern Hemisphere proxy records between 60 and 90°S (Figure 5K), and most records from north of 60 °S, show warmer conditions during the MCA (Marcott et al., 2013), yet no sustained upturn in temperature exists in the James Ross Island ice core record during the MCA and the Yanou Lake GDGT palaeotemperature record shows no significant change in the downward temperature trend initiated at c. 2.9 ka cal BP (Figure 5G, S11) (Björck et al., 1993; Mulvaney et al., 2012; Roberts et al., 2017; Kaplan et al., 2020) (Fig 5I, S12). Similarly, no evidence of substantial glacial readvance exists on KGI, northern AP region during the MCA (Charman et al., 2018; Emslie et al., 2019; Oliva et al., 2019; Kaplan et al., 2020), and marine sediment records from Maxwell Bay and Potter Cove implied no substantial increases in sea-ice (Milliken et al., 2009; Monien et al., 2011).

A readvance bulldozed marine and fluvial sediments immediately in front of the present-day BIC limits into their current positions sometime after c. 0.5 ka cal BP (68% probability) or <0.2 ka cal BP (95% probability) (Figure 3B). Hall (2007) described this as the 'last readvance' and labelled it the most extensive phase of glacier readvance of the last c. 3,500 years. The <0.2 ka readvance is broadly synchronous with geomorphological evidence for a more extensive last glacier advance across Potter Peninsula/Potter Cove from marine and terrestrial lake sediment records (Hass et al., 2010; Heredia Barión et al., submitted).

Colder conditions persisted after 0.7 ka cal BP in lake records from the mid-outer areas of Fildes Peninsula (Figure 3E) (Watcham et al., 2011; Roberts et al., 2017). The 'last readvance' is also consistent in scale and timing with the most recent glacier advance event elsewhere on the Antarctic Peninsula and on several sub-Antarctic islands (Bentley et al., 2007; Hall, 2007; Bentley et al., 2009; Hall, 2010; Roberts et al., 2010; Davies et al., 2013; Davies et al., 2014; Guglielmin et al., 2016; van der Bilt et al., 2017; Verfaillie et al., 2021), a 'post-MCA' negative phase of the SAM (Figure 7D), and several extreme cold 'events' in most Southern Hemisphere palaeorecords (Neukom et al., 2014), some of which overlap with the Northern Hemisphere 'Little Ice Age' (0.55–0.25 ka cal BP, 1,400-1,700 CE) (Mann et al., 2009; Kaufman et al., 2020).

Using radiocarbon and OSL age data obtained from raised beaches, Hall (2010) and Simms et al (2012) proposed that the rate of RSL decline accelerated following late Holocene readvance(s) sometime in the last 2,000 years. Johnson et al. (2022) published a new RSL curve that rises to maximum between 8–6 ka, with continuous decline afterwards interrupted by a possible isostatic rebound event and followed by an accelerated rate of RSL decline between 1.5–0.5 ka BP (Figure 7F) associated with the 'most significant' readvance event of the mid-late Holocene (Hall, 2010). Raised beaches <10 m a.s.l. are thought to be contemporaneous with late Holocene readvances on King George Island dated to between c. 0.5 and 0.25 ka cal BP (Sugden and John, 1973; Hall, 2010; Simms et al., 2012; Johnson et al., 2022).

A more restricted late Holocene readvance model for the Fildes Peninsula outlet of the BIC is consistent with the limited late Holocene ice-loading scenario of the W12a GIA model (Whitehouse et al., 2012a; Whitehouse et al., 2012b). Other GIA models (Simms et al., 2012) require more substantial 'Neoglacial' ice-loading, and are broadly supported by field data,

implying more substantial readvances and/or variable ice-mass (un)loading elsewhere on the South Shetland Islands during the late Holocene.

Mechanisms of Holocene glacier fluctuations

Deglaciation of the BIC on KGI to within present day limits occurred in broadly two phases during the early-mid Holocene. The first occurred between c. 15 and 8 ka cal BP, in the transition into the present interglacial (Figure 7E), driven by rising spring/summer insolation at 62 °S and elevated global solar irradiance (i.e., the power per unit area received from the Sun as measured/reconstructed on Earth) existed (Figure 7A, 7D) (Steinhilber et al., 2009; Baggenstos et al., 2019; Reynhout et al., 2019) and during a period of sustained positive (warmer) SAM-like conditions.

Longer-term changes in temperature, wind, precipitation, and sea ice formation across the NAP and SSI are primarily driven by annual to millennial scale interactions between the SHW and the SAM. Although modified by the ozone hole and other anthropogenic activities, the seasonal relationship between insolation, temperature ENSO and the SAM is thought to operate across decadal to millennial timescales during the Holocene (Perren et al., 2020). Increased cyclonic activity in the Drake Passage between 1996–2005 CE have been linked to a more poleward focussed SHW and more positive SAM. These processes drove sea-ice poleward, increasing the advection of warm air across the NAP and SSI during winter (Olivia et al., 2017; Marshall et al., 2017). Between 2006–2015 CE colder winters pushed sea ice north, increasing snowfall across the NAP and doubling snow cover on some SSI islands between 2009–14 CE (Olivia et al., 2017; de Pablo et al., 2017). As a result, the more northerly and low-lying SSI became colder, wetter and its glacier surface mass balance shifted to more positive mode (gaining mass) (Thomas et al., 2008; Goodwin et al., 2016; Oliva et al., 2017; Falk et al., 2018).

Interactions between the SAM and a deepening Amundsen Sea low have also brought warmer air from the Atlantic and north-easterly winds with cooler air from the Weddell Sea gyre in recent decades, also driving increased precipitation on the NAP and SSI (Liu et al., 2005; Davies et al., 2014; Kaplan et al., 2020). These processes are intensified in the Pacific sector that feeds into the Antarctic Peninsula by the interaction between SAM and (sub)decadal-scale changes associated with ENSO. La Niña phases of ENSO associated with colder sea surface temperatures across the eastern equatorial part of the central Pacific Ocean have been coeval with a more positive SAM (Turner et al., 2016). Conversely, positive (enhanced) phases of ENSO (El Niño) drive warmer interannual global mean temperature variability and negative phases of the SAM, with the influence of ENSO increasing over the last 4 kyr (Wang and Cai, 2013; Turner et al., 2016).

Data from the BIC foreland moraines on Fildes Peninsula, Kiteschsee Lake and comparisons to readvance constraints across KGI show that snow/ice accumulation on the BIC and smaller ice caps (e.g., Davies Heights) were sensitive to minor variations in Westerly wind strength modulated by a broad reduction in solar insolation and centennial-scale shifts in solar forcing (irradiance) during the Holocene.

Stage 1 & 2 readvances

The Stage 1 readvance occurred during a substantial (millennial scale) downturn in global solar irradiance between c. 7.5 and 7.0 ka cal BP and coincided with the transition to colder and more humid negative SAM-like conditions as the SHW migrated equatorward (Figure 7A–C, G). Consequently, glacier readvances on KGI at this time are coherent with a readvances on the eastern Antarctic Peninsula (Kaplan et al., 2020; Figure 5J) and in Patagonia at c. 7 ka (Reynhout et al., 2019).

41

Following the Stage 1 readvance on Fildes and Potter Peninsulas at c. 7 ka, the general upward trends spring/summer insolation and global solar irradiance drove further glacier retreat between 7 and 6 ka cal BP (Figure 5A). Glacier retreat on Fildes Peninsula and Potter Peninsula at c. 6.0 ka cal BP coincided with sustained temperatures above 12 ka mean in the Southern Hemisphere high latitudes and the 'Holocene global thermal maximum', centred on 6.5–6.0 ka cal BP, which was, globally, 0.7 °C warmer than the pre-industrial 19th Century (Kaufman et al., 2020) (Figure 5K). Glaciers on King George Island were maintained at or around their Stage 1 readvance positions until at least c. 6.5 ka, when reducing solar irradiance and weaker Westerlies c. 54°S and reduced storminess over the South Shetlands Islands prevailed as the core SHW belt shifted further equatorward (Figure 7A-D, G, H) (Bentley et al., 2009; Quade and Kaplan, 2017; Saunders et al., 2018; Reynhout et al., 2019; Heredia Barión et al., submitted). Probability 'gaps' when Stage 2 readvances could have occurred between 6-3.5 ka coincide with phases of increased SHW (Figure 7B).

Stage 3 and 4 readvances

The late Holocene Stage 3 readvance (1.7–1.4 ka cal BP on Fildes Peninsula) coincided with a gradual decline in spring/summer insolation at 62°S and millennial-centennial scale fluctuations irradiance, colder/wetter negative SAM-like conditions and enhanced Westerly winds and an increasing ENSO from c. 4 ka onwards drove the regional-hemispheric deterioration in climatic conditions initiated after 2070 ± 50 cal BP (Čejka et al., 2020) (Figure 5F-G, 7, S12). Dating errors notwithstanding, Stage 3 and 4 readvances of the BIC appear to be associated with two short-lived transitions to more positive SAM-like conditions (Figure 7A-D, G, H), which could have led to increased snow accumulation on and readvance of the BIC (Garreaud, 2007; Yang et al., 2019), sustaining glaciers and increasing turbidity in Kiteschsee Lake (Figure 4, 5B).

From the mid-late C20[th] onwards, the mode of sedimentation in Kiteschsee Lake and other lakes on Fildes Peninsula and King George Island has shifted dramatically to one dominated by aquatic moss (Figure 4A, S1). We link this final ecological shift to the Recent Rapid Warming (RRR) of Bentley et al., (2009). The dramatic shift to increasingly positive SAM-like conditions (Figure 7D) in late C20[th] and early C21[st] climate data (Marshall, 2007) has been linked to the ozone hole, increasing greenhouse gas emissions, and warmer global temperatures, and has drawn stronger Westerly winds closer to the Antarctic continent.

To summarise, new probability density phase modelling shows that early-mid Holocene readvances on the South Shetland Islands occurred mainly during colder/ more humid negative SAM-like conditions. From c. 5 ka onwards, more intense SHW and prolonged phases of negative SAM-like prevailed and drove restricted readvances of the BIC on Fildes Peninsula phases of reduced solar irradiance. Overall, three of the four readvance phases (Stages 1, 3, 4) were initiated in phases of reduced solar irradiance, which would have lowered the ELA on the SSI. Similarities in the timing of glacier readvances across most of the mid-late Holocene and millennial scale connections between the Antarctic Peninsula, South America and sub-Antarctic Islands imply underlying regional-hemispheric driving mechanisms, such as the SHW SAM as driving mechanisms.

Conclusions

We reconstructed the mid–late Holocene deglaciation and readvance history of northern Fildes Peninsula using a combination of new cosmogenic exposure ages from glacial erratics on the foreland of the Bellingshausen Ice Cap (BIC), radiocarbon dating of terrestrial mosses and marine *Laternula* sp. bivalve shells found in moraines on the Artigas Beach and Valle Norte sectors of BIC foreland, and multi-proxy analyses of lake sediments from Kiteschsee Lake. We used probability density phase modelling to help refine the chronology of mid–late Holocene

glacier readvances of the Bellingshausen Ice Cap (BIC) on the Fildes Peninsula and elsewhere on King George Island. We established the following four-stage readvance model, with up to eight probability 'gaps' where readvances could have occurred:

Stage 1 readvance, c. 7.4–6.6 ka cal BP: After deglaciation during a prolonged phase of positive SAM-like conditions in the early Holocene warmth, a minor glacier readvance occurred during a regional-hemispheric cooler/wetter negative SAM phase and a phase of reduced global solar irradiance between c. 7.5 and 7.0 ka cal BP. After 6.6 ka cal BP, spring/summer insolation at 62 °S gradually increased and regional temperatures reached their mid-late Holocene maximum. The north-western marine platform, at c. 40–35 m a.s.l. became ice-free, and the BIC retreated to a similar configuration to the present day on Fildes Peninsula between c. 6.6–5.3 ka cal BP.

Stage 2 readvances, c. 5.3–2.2 ka cal BP: We found no new evidence for glacier readvance beyond present day limits on Fildes Peninsula, but identified up to four probability 'gaps' where readvances could have occurred exist between 5.3–4.8, 4.5–3.9, 3.3–3.0, 2.6–2.2 ka cal BP.

Stage 3 readvance, c. 1.7–1.5 ka cal BP: Terrestrial mosses in the Shetland I moraine suggest that the BIC extended landward of its present position on its eastern flank during a shift to colder 'Neoglacial' conditions across the Antarctic Peninsula after c. 2.0 ka cal BP as spring/summer insolation at 62 °S decreased.

Stage 4 readvances c. 1.3–0.7 and <0.7 ka cal BP: Regional 'Neoglacial' conditions persisted on the South Shetland Islands as spring/summer insolation at 62 °S continued its downward trend. Moss fragments and mid Holocene marine sediments were translocated into the moraines

surrounding the present-day BIC between c. 1.3–0.7 ka and prolonged phase of elevated turbidity existed in Kiteschsee Lake. Previous studies showed the BIC readvance after c. 0.7 ka cal BP and was the most extensive of readvance of the last 3,500 years (Hall, 2007). The timing overlaps broadly with the timing of the Northern Hemisphere 'Little Ice Age' and is consistent with geomorphological and marine sediment core evidence for an extensive last glacier advance in Potter Peninsula/Cove and on James Ross Island, NE Antarctic Peninsula. This 'last readvance' was likely driven the continuing downturn trend in spring/summer solar insolation at 62 °S, a centennial-scale solar forcing (irradiance) minimum, coupled with a return to more negative (cold, humid) SAM-like conditions on the SSI and northern Antarctic Peninsula. Recovery from late Holocene 'Neoglacial' conditions during the mid–late C20th onwards was characterised in Kiteschsee Lake and other lakes on Fildes Peninsula by the re-colonisation of thick aquatic moss at the lake sediment-water interface. This shift was likely driven by late 20th Century/early 21st Century warming of the Antarctic Peninsula and the transition to increasingly more positive SAM-like conditions.

45

Funding

Author Contributions

PHB and SR designed the research and wrote the manuscript, constructed figures and tables with assistance from JD, IG, MB, GK; PHB, SR, EP, MB, DH, EH undertook fieldwork/sample collection. PHB and SB produced cosmogenic nuclide dating data; while CS provided [10]Be exposure dating analytical facilities; PHB, LW, GK, SR, MB undertook radiocarbon dating. Kiteschsee Lake core data and interpretations were undertaken by SR, EP, SD (ITRAX-XRF), JD, VJ (diatom analysis) IG, SB, RM, CH (tephra counting, geochemical identification of tephra layers); PHB, SR, CS, SB, GK, EP, MB, JS edited initial drafts and all authors read and commented on the final version. The authors declare no competing interests.

Data availability

Key datasets generated in this study are included in the main text and Supplementary Materials: https://doi.org/10.6084/m9.figshare.21352569.v1. All code, data, packages and package references, can be found at: https://github.com/stever60/Fildes_Peninsula. Data can be obtained from the NERC EDS UK Polar Data Centre (PDC) as follows (PDC doi assignments pending): Chronological data: https://github.com/stever60/Fildes_Peninsula;

Lake sediment data: https://github.com/stever60/Fildes_Peninsula;

Advance/retreat data: https://github.com/stever60/Fildes_Peninsula

They are also available on request from the Polar Data Centre (polardatacentre@bas.ac.uk), PHB (herediabarionpablo@yahoo.com.ar) and SR (sjro@bas.ac.uk).

References

Antoniades D, Giralt S, Geyer A, Álvarez-Valero AM, Pla-Rabes S, Granados I, et al. (2018) The timing and widespread effects of the largest Holocene volcanic eruption in Antarctica. *Scientific Reports* 8: 17279.

Ariztegui D, Gilli A, Anselmetti FS, Goñi RA, Belardi JB and Espinosa S. (2010) Lake-level changes in central Patagonia (Argentina): crossing environmental thresholds for Lateglacial and Holocene human occupation. *Journal of Quaternary Science* 25: 1092-1099.

Baggenstos D, Häberli M, Schmitt J, Shackleton SA, Birner B, Severinghaus JP, et al. (2019) Earth's radiative imbalance from the Last Glacial Maximum to the present. *Proceedings of the National Academy of Sciences* 116: 14881-14886.

Balco G. (2011) Contributions and unrealized potential contributions of cosmogenic-nuclide exposure dating to glacier chronology, 1990–2010. *Quaternary Science Reviews* 30: 3-27.

Balco G and Schaefer JM. (2013) Exposure-age record of Holocene ice sheet and ice shelf change in the northeast Antarctic Peninsula. *Quaternary Science Reviews* 59: 101-111.

Balco G, Stone JO, Lifton NA and Dunai TJ. (2008) A complete and easily accessible means of calculating surface exposure ages or erosion rates from 10Be and 26Al measurements. *Quaternary Geochronology* 3: 174-195.

Bañón M, Justel A, Velázquez D and Quesada A. (2013) Regional weather survey on Byers Peninsula, Livingston Island, South Shetland Islands, Antarctica. *Antarctic Science* 25: 146-156.

Barsch D and Mäusbacher R. (1986) New Data on the Relief Development of the South Shetland Islands, Antarctica. *Interdisciplinary Science Reviews* 11: 211-218.

Bentley MJ, Hodgson DA, Smith JA and Cox NJ. (2005) Relative sea level curves for the South Shetland Islands and Marguerite Bay, Antarctic Peninsula. Quaternary Science Reviews 24: 1203-1216.

Bentley MJ, Evans DJA, Fogwill CJ, Hansom JD, Sugden DE and Kubik PW. (2007) Glacial geomorphology and chronology of deglaciation, South Georgia, sub-Antarctic. *Quaternary Science Reviews* 26: 644-677.

Bentley MJ, Hodgson DA, Smith JA, Cofaigh CÓ, Domack EW, Larter RD, et al. (2009) Mechanisms of Holocene palaeoenvironmental change in the Antarctic Peninsula region. *The Holocene* 19: 51-69.

Bevan A. (2021) rcarbon: Calibration and Analysis of Radiocarbon Dates. *https://github.com/ahb108/rcarbon/*.

Binnie SA, Dunai TJ, Voronina E, Goral T, Heinze S and Dewald A. (2015) Separation of Be and Al for AMS using single-step column chromatography. *Nuclear Instruments and Methods in Physics Research Section B: Beam Interactions with Materials and Atoms* 361: 397-401.

Björck S, Håkansson H, Olsson S, Barnekow L and Janssens J. (1993) Palaeoclimatic studies in South Shetland Islands, Antarctica, based on numerous stratigraphic variables in lake sediments. *Journal of Paleolimnology* 8: 233-272.

Björck S, Hjort, C., Ingolfsson, O., Skog, G. (1991a) Radiocarbon dates from the Antarctic Peninsula region — problems and potential. In: Lowe JJ (ed) *Radiocarbon dating: recent applications and future potential.* Quaternary Proceedings 1: 55–65.

Björck S, Nils Malmer, Christian Hjort, Per Sandgren, Ólafur Ingólfsson, Bo Wallén, Ronald Ian Lewis Smith, and Bodil Liedberg Jónsson. (1991b) Stratigraphic and Paleoclimatic Studies of a 5500-Year-Old Moss Bank on Elephant Island, Antarctica. *Arctic and Alpine Research* 23: 361-374.

Blaauw M and Christen JA. (2011) Flexible paleoclimate age-depth models using an autoregressive gamma process. *Bayesian Analysis* 6: 457-474.

Blockley SPE, Pyne-O'Donnell SDF, Lowe JJ, Matthews IP, Stone A, Pollard AM, et al. (2005) A new and less destructive laboratory procedure for the physical separation of distal glass tephra shards from sediments. *Quaternary Science Reviews* 24: 1952-1960.

Borchers B, Marrero S, Balco G, Caffee M, Goehring B, Lifton N, et al. (2016) Geological calibration of spallation production rates in the CRONUS-Earth project. *Quaternary Geochronology* 31: 188-198.

Bronk Ramsey C. (2009) Bayesian Analysis of Radiocarbon Dates. *Radiocarbon* 51: 337-360.

Čejka T, Nývlt D, Kopalová K, Bulínová M, Kavan J, Lirio JM, et al. (2020) Timing of the neoglacial onset on the North-Eastern Antarctic Peninsula based on lacustrine archive from Lake Anónima, Vega Island. *Global and Planetary Change* 184: 103050.

Charman DJ, Amesbury MJ, Roland TP, Royles J, Hodgson DA, Convey P, et al. (2018) Spatially coherent late Holocene Antarctic Peninsula surface air temperature variability. *Geology* 46: 1071-1074.

Christeson GL, Barker DHN, Austin Jr. JA and Dalziel IWD. (2003) Deep crustal structure of Bransfield Strait: Initiation of a back arc basin by rift reactivation and propagation. *Journal of Geophysical Research: Solid Earth* 108.

Chu Z, Sun L, Wang Y, Huang T and Zhou X. (2017) Depositional environment and climate changes during the Holocene in Grande Valley, Fildes Peninsula, King George Island, Antarctica. *Antarctic Science* 29: 545-554.

Cole-Dai J, Ferris DG, Kennedy JA, Sigl M, McConnell JR, Fudge TJ, et al. (2021) Comprehensive Record of Volcanic Eruptions in the Holocene (11,000 years) From the WAIS Divide, Antarctica Ice Core. *Journal of Geophysical Research: Atmospheres* 126: e2020JD032855.

Davies BJ, Glasser NF, Carrivick JL, Hambrey MJ, Smellie JL and Nývlt D. (2013) Landscape evolution and ice-sheet behaviour in a semi-arid polar environment: James Ross Island, NE Antarctic Peninsula. *Geological Society, London, Special Publications* 381: 353-395.

Davies BJ, Golledge NR, Glasser NF, Carrivick JL, Ligtenberg SRM, Barrand NE, et al. (2014) Modelled glacier response to centennial temperature and precipitation trends on the Antarctic Peninsula. *Nature Climate Change* 4: 993-998.

Davies BJ, Hambrey MJ, Glasser NF, Holt T, Rodés A, Smellie JL, et al. (2017) Ice-dammed lateral lake and epishelf lake insights into Holocene dynamics of Marguerite Trough Ice Stream and George VI Ice Shelf, Alexander Island, Antarctic Peninsula. *Quaternary Science Reviews* 177: 189-219.

Davies SJ, Lamb HF and Roberts SJ. (2015) Micro-XRF Core Scanning in Palaeolimnology: Recent Developments. In: Croudace IW and Rothwell RG (eds) *Micro-XRF Studies of Sediment Cores: Applications of a non-destructive tool for the environmental sciences.* Dordrecht: Springer Netherlands, 189-226.

de Pablo MA, Blanco JJ, Molina A, Ramos M, Quesada A and Vieira G. (2013) Interannual active layer variability at the Limnopolar Lake CALM site on Byers Peninsula, Livingston Island, Antarctica. *Antarctic Science* 25: 167-180.

Emslie SD, Romero M, Juáres MA and Argota MR. (2019) Holocene occupation history of pygoscelid penguins at Stranger Point, King George (25 de Mayo) Island, northern Antarctic Peninsula. *The Holocene*: 0959683619875814.

Etourneau J, Collins LG, Willmott V, Kim JH, Barbara L, Leventer A, et al. (2013) Holocene climate variations in the western Antarctic Peninsula: evidence for sea ice extent predominantly controlled by changes in insolation and ENSO variability. *Climate of the Past* 9: 1431-1446.

Falk U, López DA and Silva-Busso A. (2018) Multi-year analysis of distributed glacier mass balance modelling and equilibrium line altitude on King George Island, Antarctic Peninsula. *The Cryosphere* 12: 1211-1232.

Foster LC, Pearson EJ, Juggins S, Hodgson DA, Saunders KM, Verleyen E, et al. (2016) Development of a regional glycerol dialkyl glycerol tetraether (GDGT)–temperature calibration for Antarctic and sub-Antarctic lakes. *Earth and Planetary Science Letters* 433: 370-379.

Fretwell PT, Hodgson DA, Watcham EP, Bentley MJ and Roberts SJ. (2010) Holocene isostatic uplift of the South Shetland Islands, Antarctic Peninsula, modelled from raised beaches. *Quaternary Science Reviews* 29: 1880-1893.

Gabriel I, Roberts SJ, McCulloch RDM, Hayward CL, Davies SJ, Pearson EP, et al. (2021 submitted) New evidence of multiple rhyolitic tephra deposits in lake sediments from King George Island, NW Antarctic Peninsula *The Holocene.*

Garreaud R. (2007) Precipitation and Circulation Covariability in the Extratropics. *Journal of Climate* 20: 4789-4797.

Glasser NF, Davies BJ, Carrivick JL, Rodés A, Hambrey MJ, Smellie JL, et al. (2014) Ice-stream initiation, duration and thinning on James Ross Island, northern Antarctic Peninsula. *Quaternary Science Reviews* 86: 78-88.

Goodwin BP, Mosley-Thompson E, Wilson AB, Porter SE and Sierra-Hernandez MR. (2016) Accumulation Variability in the Antarctic Peninsula: The Role of Large-Scale Atmospheric Oscillations and Their Interactions. *Journal of Climate* 29: 2579-2596.

Guglielmin M, Convey P, Malfasi F and Cannone N. (2016) Glacial fluctuations since the 'Medieval Warm Period' at Rothera Point (western Antarctic Peninsula). *The Holocene* 26: 154-158.

Hall, B.L. (2003). An Overview of Late Pleistocene Glaciation in the South Shetland Islands. In E. Domack, A. Levente, A. Burnet, et al. (eds) *Antarctic Peninsula Climate Variability: Historical and Paleoenvironmental Perspectives.* American Geophysical Union: 10.1029/AR079p0103

Hall BL. (2007) Late-Holocene advance of the Collins Ice Cap, King George Island, South Shetland Islands. *The Holocene* 17: 1253-1258.

Hall BL. (2009) Holocene glacial history of Antarctica and the sub-Antarctic islands. *Quaternary Science Reviews* 28: 2213-2230.

Hall BL. (2010) Holocene relative sea-level changes and ice fluctuations in the South Shetland Islands. *Global and Planetary Change* 74: 15-26.

Haslett J and Parnell A. (2008) A simple monotone process with application to radiocarbon-dated depth chronologies. *Journal of the Royal Statistical Society: Series C (Applied Statistics)* 57: 399-418.

Hass HC, Kuhn G, Monien P, Brumsack H-J and Forwick M. (2010) Climate fluctuations during the past two millennia as recorded in sediments from Maxwell Bay, South Shetland Islands, West Antarctica. *Geological Society, London, Special Publications* 344: 243-260.

Heaton TJ, Köhler P, Butzin M, Bard E, Reimer RW, Austin WEN, et al. (2020) Marine20—The Marine Radiocarbon Age Calibration Curve (0–55,000 cal BP). *Radiocarbon* 62: 779-820.

Hein AS, Marrero SM, Woodward J, Dunning SA, Winter K, Westoby MJ, et al. (2016) Mid-Holocene pulse of thinning in the Weddell Sea sector of the West Antarctic ice sheet. *Nature Communications* 7: 12511.

Heredia Barión PA, Strelin JA, Roberts SJ, Spiegel C, Wacker L, Niedermann S, et al. (submitted) The impact of Holocene deglaciation and glacial dynamics on the landscapes and geomorphology of Potter Peninsula, King George Island (Isla 25 Mayo), NW Antarctic Peninsula. https://doi.org/10.6084/m9.figshare.21352881.v1

Hogg AG, Heaton TJ, Hua Q, Palmer JG, Turney CSM, Southon J, et al. (2020) SHCal20 Southern Hemisphere Calibration, 0–55,000 Years cal BP. *Radiocarbon* 62: 759-778.

Hogg AG, Hua Q, Blackwell PG, Niu M, Buck CE, Guilderson TP, et al. (2013) SHCal13 Southern Hemisphere Calibration, 0–50,000 Years cal BP. *Radiocarbon* 55: 1889-1903.

Ingólfsson Ó, Hjort C and Humlum O. (2003) Glacial and Climate History of the Antarctic Peninsula since the Last Glacial Maximum. *Arctic, Antarctic, and Alpine Research* 35: 175-186.

John BS and Sugden DE. (1971) Raised marine features and phases of glaciation in the South Shetland Islands. *British Antarctic Survey Bulletin* 24: 45-111.

Johnson JS, Bentley MJ, Roberts SJ, Binnie SA and Freeman SPHT. (2011) Holocene deglacial history of the northeast Antarctic Peninsula – A review and new chronological constraints. *Quaternary Science Reviews* 30: 3791-3802.

Johnson JS, Everest JD, Leat PT, Golledge NR, Rood DH and Stuart FM. (2012) The deglacial history of NW Alexander Island, Antarctica, from surface exposure dating. *Quaternary Research* 77: 273-280.

Johnson JS, Roberts SJ, Rood DH, Pollard D, Schaefer JM, Whitehouse PL, et al. (2020) Deglaciation of Pope Glacier implies widespread early Holocene ice sheet thinning in the Amundsen Sea sector of Antarctica. *Earth and Planetary Science Letters* 548: 116501.

Johnson JS, Smith JA, Schaefer JM, Young NE, Goehring BM, Hillenbrand C-D, et al. (2017) The last glaciation of Bear Peninsula, central Amundsen Sea Embayment of Antarctica: Constraints on timing and duration revealed by in situ cosmogenic 14C and 10Be dating. *Quaternary Science Reviews* 178: 77-88.

Johnson JS, Venturelli RA, Balco G, Allen CS, Braddock S, Campbell S, et al. (2022) Review article: Existing and potential evidence for Holocene grounding line retreat and readvance in Antarctica. *The Cryosphere* 16: 1543-1562.

Jones VJ and Juggins S. (1995) The construction of a diatom-based chlorophyll a transfer function and its application at three lakes on Signy Island (maritime Antarctic) subject to differing degrees of nutrient enrichment. *Freshwater Biology* 34: 433-445.

Juggins S. (2007) C2 Version 1.5 User Guide. Software for ecological and palaeoecological data analysis and visualisation. Newcastle University.

Juggins S. (2012) Rioja: Analysis of Quaternary Science Data, R package version (0.8-5).

Kaplan MR, Strelin JA, Schaefer JM, Denton GH, Finkel RC, Schwartz R, et al. (2011) In-situ cosmogenic 10Be production rate at Lago Argentino, Patagonia: Implications for late-glacial climate chronology. *Earth and Planetary Science Letters* 309: 21-32.

Kaplan MR, Strelin JA, Schaefer JM, Peltier C, Martini MA, Flores E, et al. (2020) Holocene glacier behavior around the northern Antarctic Peninsula and possible causes. *Earth and Planetary Science Letters* 534: 116077.

Kaufman D, McKay N, Routson C, Erb M, Davis B, Heiri O, et al. (2020) A global database of Holocene paleotemperature records. *Scientific Data* 7: 115.

Kejna M, Araźny A and Sobota I. (2013) Climatic change on King George Island in the years 1948–2011. *Polish Polar Research* 34: 213-235.

King JC and Turner J. (1997) *Antarctic Meteorology and Climatology*. Cambridge: Cambridge University Press.

Kohl CP and Nishiizumi K. (1992) Chemical isolation of quartz for measurement of in-situ -produced cosmogenic nuclides. *Geochimica et Cosmochimica Acta* 56: 3583-3587.

Lacourse T and Gajewski K. (2020) Current practices in building and reporting age-depth models. *Quaternary Research* 96: 28-38.

Lamb HH. (1965) The early medieval warm epoch and its sequel. *Palaeogeography, Palaeoclimatology, Palaeoecology* 1: 13-37.

Lamy F, Kilian R, Arz HW, Francois J-P, Kaiser J, Prange M, et al. (2010) Holocene changes in the position and intensity of the southern westerly wind belt. *Nature Geoscience* 3: 695.

Laskar J, Robutel P, Joutel F, Gastineau M, Correia ACM and Levrard B. (2004) A long-term numerical solution for the insolation quantities of the Earth. *A&A* 428: 261-285.

Lifton N. (2016) Implications of two Holocene time-dependent geomagnetic models for cosmogenic nuclide production rate scaling. *Earth and Planetary Science Letters* 433: 257-268.

Lifton N, Sato T and Dunai TJ. (2014) Scaling in situ cosmogenic nuclide production rates using analytical approximations to atmospheric cosmic-ray fluxes. *Earth and Planetary Science Letters* 386: 149-160.

Lindow J, Castex M, Wittmann H, Johnson JS, Lisker F, Gohl K, et al. (2014) Glacial retreat in the Amundsen Sea sector, West Antarctica – first cosmogenic evidence from central Pine Island Bay and the Kohler Range. *Quaternary Science Reviews* 98: 166-173.

Liu XD, Sun LG, Xie ZQ, Yin XB and Wang YH. (2005) A 1300-year record of penguin populations at Ardley Island in the Antarctic, as deduced from the geochemical data in the ornithogenic lake sediments. *Arctic Antarctic and Alpine Research* 37: 490-498.

Mann ME, Steinman BA, Brouillette DJ and Miller SK. (2021) Multidecadal climate oscillations during the past millennium driven by volcanic forcing. *Science* 371: 1014.

Mann ME, Zhang Z, Rutherford S, Bradley RS, Hughes MK, Shindell D, et al. (2009) Global Signatures and Dynamical Origins of the Little Ice Age and Medieval Climate Anomaly. *Science* 326: 1256-1260.

Marcott SA, Shakun JD, Clark PU and Mix AC. (2013) A Reconstruction of Regional and Global Temperature for the Past 11,300 Years. *Science* 339: 1198-1201.

Marshall GJ. (2007) Half-century seasonal relationships between the Southern Annular mode and Antarctic temperatures. *International Journal of Climatology* 27: 373-383.

Marshall GJ, Thompson DWJ and van den Broeke MR. (2017) The Signature of Southern Hemisphere Atmospheric Circulation Patterns in Antarctic Precipitation. *Geophysical Research Letters* 44: 11,580-511,589.

Martin MA, Azorin Molina C, Utrabo Carazo E, Bedoya Valestt S and Guijarro JA. (2021) Wind speed variability over the South Shetland Islands, 1988-2019: the relationship between easterlies winds and SAM. EGU21-8706.

Masson V, Vimeux F, Jouzel J, Morgan V, Delmotte M, Ciais P, et al. (2000) Holocene Climate Variability in Antarctica Based on 11 Ice-Core Isotopic Records. *Quaternary Research* 54: 348-358.

Mäusbacher R. (1991) Die jungquartare Relief- und Klimageschichte im Bereich der Fildeshalbinsel Süd-Shetland Inseln, Antarktis. *Heidelberger Geographischen Arbeiten.* Geographischen Instituts der Universitat Heidelberg: Heidelberg.

Mäusbacher R, Müller J and Schmidt R. (1989) Evolution of postglacial sedimentation in Antarctic lakes (King George Island). *Zeitschrift für Geomorphologie* 33: 219–234.

Meredith MP and King JC. (2005) Rapid climate change in the ocean west of the Antarctic Peninsula during the second half of the 20th century. *Geophysical Research Letters* 32: doi:10.1029/2005GL024042.

Michel RFM, Schaefer CEGR, Simas FMB, Francelino MR, Fernandes-Filho EI, Lyra GB, et al. (2014) Active-layer thermal monitoring on the Fildes Peninsula, King George Island, maritime Antarctica. *Solid Earth* 5: 1361-1374.

Milliken KT, Anderson JB, Wellner JS, Bohaty SM and Manley PL. (2009) High-resolution Holocene climate record from Maxwell Bay, South Shetland Islands, Antarctica. *Geological Society of America Bulletin* 121: 1711-1725.

Monien P, Schnetger B, Brumsack H-J, Hass HC and Kuhn G. (2011) A geochemical record of late Holocene palaeoenvironmental changes at King George Island (maritime Antarctica). *Antarctic Science* 23: 255-267.

Moreno PI, Vilanova I, Villa-Martínez R, Dunbar RB, Mucciarone DA, Kaplan MR, et al. (2018) Onset and Evolution of Southern Annular Mode-Like Changes at Centennial Timescale. *Scientific Reports* 8: 3458.

Moreno PI, Henríquez WI, Pesce OH, Henríquez CA, Fletcher MS, Garreaud RD, et al. (2021) An early Holocene westerly minimum in the southern mid-latitudes. *Quaternary Science Reviews* 251: 106730.

Moy CM, Dunbar RB, Moreno PI, Francois J-P, Villa-Martínez R, Mucciarone DM, et al. (2008) Isotopic evidence for hydrologic change related to the westerlies in SW Patagonia, Chile, during the last millennium. *Quaternary Science Reviews* 27: 1335-1349.

Mulvaney R, Abram NJ, Hindmarsh RCA, Arrowsmith C, Fleet L, Triest J, et al. (2012) Recent Antarctic Peninsula warming relative to Holocene climate and ice-shelf history. *Nature* 489: 141-144.

Neukom R, Gergis J, Karoly DJ, Wanner H, Curran M, Elbert J, et al. (2014) Inter-hemispheric temperature variability over the past millennium. *Nature Clim. Change* 4: 362-367.

Ó Cofaigh C, Davies BJ, Livingstone SJ, Smith JA, Johnson JS, Hocking EP, et al. (2014) Reconstruction of ice-sheet changes in the Antarctic Peninsula since the Last Glacial Maximum. *Quaternary Science Reviews* 100: 87-110.

Oksanen J. (2014) Vegan: Community Ecology Package. R package version 2.3-0. http://cran.r-project.org/web/packages/vegan/index.html.

Oliva M, Antoniades D, Serrano E, Giralt S, Liu EJ, Granados I, et al. (2019) The deglaciation of Barton Peninsula (King George Island, South Shetland Islands, Antarctica) based on geomorphological evidence and lacustrine records. *Polar Record* 55: 177-188.

Oliva M, Mercier D, Ruiz-Fernández J and McColl S. (2020) Paraglacial processes in recently deglaciated environments. *Land Degradation & Development* 31: 1871-1876.

Oliva M, Navarro F, Hrbáček F, Hernández A, Nývlt D, Pereira P, et al. (2017) Recent regional climate cooling on the Antarctic Peninsula and associated impacts on the cryosphere. *Science of The Total Environment* 580: 210-223.

Palacios D, Ruiz-Fernández J, Oliva M, Andrés N, Fernández-Fernández JM, Schimmelpfennig I, et al. (2020) Timing of formation of neoglacial landforms in the South Shetland Islands (Antarctic Peninsula): Regional and global implications. *Quaternary Science Reviews* 234: 106248.

Pallàs R, James T, Sàbat F, Vilaplana J, Grant D and Ricci C. (1997) Holocene uplift in the South Shetland Islands: evaluation of tectonics and glacio-isostasy. In: Ricci C (ed) The Antarctic Region: Geological Evolution and Processes. Siena, Italy: Terra Antarctica Publication, 861–868.

Parnell AC. (2021) Bchron: Radiocarbon Dating, Age-Depth Modelling, Relative Sea Level Rate Estimation, and Non-Parametric Phase Modelling. *https://github.com/andrewcparnell/Bchron/*.

Perren BB, Hodgson DA, Roberts SJ, Sime L, Van Nieuwenhuyze W, Verleyen E, et al. (2020) Southward migration of the Southern Hemisphere westerly winds corresponds with warming climate over centennial timescales. *Communications Earth & Environment* 1: 58.

Putnam AE, Schaefer JM, Barrell DJA, Vandergoes M, Denton GH, Kaplan MR, et al. (2010) In situ cosmogenic 10Be production-rate calibration from the Southern Alps, New Zealand. *Quaternary Geochronology* 5: 392-409.

Quade J and Kaplan MR. (2017) Lake-level stratigraphy and geochronology revisited at Lago (Lake) Cardiel, Argentina, and changes in the Southern Hemispheric Westerlies over the last 25 ka. *Quaternary Science Reviews* 177: 173-188.

Reynhout SA, Sagredo EA, Kaplan MR, Aravena JC, Martini MA, Moreno PI, et al. (2019) Holocene glacier fluctuations in Patagonia are modulated by summer insolation intensity and paced by Southern Annular Mode-like variability. *Quaternary Science Reviews* 220: 178-187.

Roberts SJ, Hodgson DA, Bentley MJ, Smith JA, Millar IL, Olive V, et al. (2008) The Holocene history of George VI Ice Shelf, Antarctic Peninsula from clast-provenance analysis of epishelf lake sediments. *Palaeogeography Palaeoclimatology Palaeoecology* 259: 258-283.

Roberts SJ, Hodgson DA, Shelley S, Royles J, Griffiths HJ, Deen TJ, et al. (2010) Establishing Lichenometric Ages for Nineteenth- and Twentieth-Century Glacier Fluctuations on South Georgia (South Atlantic). *Geografiska Annaler Series a-Physical Geography* 92A: 125-139.

Roberts SJ, Hodgson DA, Sterken M, Whitehouse PL, Verleyen E, Vyverman W, et al. (2011) Geological constraints on glacio-isostatic adjustment models of relative sea-level change during deglaciation of Prince Gustav Channel, Antarctic Peninsula. *Quaternary Science Reviews* 30: 3603-3617.

Roberts SJ, Monien P, Foster LC, Loftfield J, Hocking EP, Schnetger B, et al. (2017) Past penguin colony responses to explosive volcanism on the Antarctic Peninsula. *Nature Communications* 8: 14914.

Saunders KM, Roberts SJ, Perren B, Butz C, Sime L, Davies S, et al. (2018) Holocene dynamics of the Southern Hemisphere westerly winds and possible links to CO2 outgassing. *Nature Geoscience* 11: 650-655.

Schmidt R, Mäusbacher R and Müller J. (1990) Holocene diatom flora and stratigraphy from sediment cores of two Antarctic lakes (King George Island). *Journal of Paleolimnology* 3: 55-74.

Seong YB, Owen LA, Lim HS, Yoon HI, Kim Y, Lee YI, et al. (2008) Rate of late Quaternary ice-cap thinning on King George Island, South Shetland Islands, West Antarctica defined by cosmogenic 36Cl surface exposure dating. *Boreas* 38: 207-213.

Seong YB, Owen LA, Lim HS, Yoon HI, Kim Y, Lee YI, et al. (2009) Rate of late Quaternary ice-cap thinning on King George Island, South Shetland Islands, West Antarctica defined by cosmogenic 36Cl surface exposure dating. *Boreas* 38: 207-213.

Simms AR, Milliken KT, Anderson JB and Wellner JS. (2011) The marine record of deglaciation of the South Shetland Islands, Antarctica since the Last Glacial Maximum. *Quaternary Science Reviews* 30: 1583-1601.

Simms AR, Ivins ER, DeWitt R, Kouremenos P and Simkins LM. (2012) Timing of the most recent Neoglacial advance and retreat in the South Shetland Islands, Antarctic Peninsula: insights from raised beaches and Holocene uplift rates. *Quaternary Science Reviews* 47: 41-55.

Simms AR, Lisiecki L, Gebbie G, Whitehouse PL and Clark JF. (2019) Balancing the last glacial maximum (LGM) sea-level budget. *Quaternary Science Reviews* 205: 143-153.\

Simms AR, Bentley MJ, Simkins LM, Zurbuchen J, Reynolds LC, DeWitt R, et al. (2021) Evidence for a "Little Ice Age" glacial advance within the Antarctic Peninsula – Examples from glacially-overrun raised beaches. Quaternary Science Reviews 271: 107195.

Smellie JL, Pankhurst R, Thomson MRA and Davies RES. (1984) The geology of the South Shetland Islands: VI. Stratigraphy, geochemistry and evolution. *British Antarctic Survey Scientific Reports* 87: 85 pp.

Steinhilber F, Beer J and Fröhlich C. (2009) Total solar irradiance during the Holocene. *Geophysical Research Letters* 36: L19704.

Stone JO. (2000) Air pressure and cosmogenic isotope production. *Journal of Geophysical Research: Solid Earth* 105: 23753-23759.

Strelin JA, Kaplan MR, Vandergoes MJ, Denton GH and Schaefer JM. (2014) Holocene glacier history of the Lago Argentino basin, Southern Patagonian Icefield. *Quaternary Science Reviews* 101: 124-145.

Sugden DE and Clapperton CM. (1977) The maximum ice extent on island groups in the Scotia sea, Antarctica. *Quaternary Research* 7: 268-282.

Sugden DE and John BS. (1973) The ages of glacier fluctuations in the South Shetland Islands, Antarctica. In: van Zinderen; Bakker EM (ed) *Palaeoecology of Africa, the Surrounding Islands and Antarctica.* Balkema, Cape Town, 141-159.

Sun LG, Liu XD, Yin XB, Xie ZQ and Zhao JL. (2005) Sediments in palaeo-notches: potential proxy records for palaeoclimatic changes in Antarctica. *Palaeogeography, Palaeoclimatology, Palaeoecology* 218: 175-193.

Tatur A, Martinez-Macchiavello JC, Niegodzisz J and del Valle R. (1999) A record of Holocene environmental changes in sediment core of Hotel Lake, King George Island, Antarctica. *Polish Polar Studies* 26 Polar Symposium.

Thomas ER, Marshall GJ and McConnell JR. (2008) A doubling in snow accumulation in the western Antarctic Peninsula since 1850. *Geophysical Research Letters* 35: L01706.

Turner J, Lachlan-Cope TA, Marshall GJ, et al. (2002) Spatial variability of Antarctic Peninsula net surface mass balance. *Journal of Geophysical Research: Atmospheres* 107: AAC 4-1-AAC 4-18.

Turner J, Colwell SR, Marshall GJ, Lachlan-Cope TA, Carleton AM, Jones PD, et al. (2004) The SCAR READER Project: Toward a High-Quality Database of Mean Antarctic Meteorological Observations. *Journal of Climate* 17: 2890-2898.

Turner J, Lu H, White I, King JC, Phillips T, Hosking JS, et al. (2016) Absence of 21st century warming on Antarctic Peninsula consistent with natural variability. *Nature* 535: 411-415.

van der Bilt WGM, Bakke J, Werner JP, Paasche Ø, Rosqvist G and Vatle SS. (2017) Late Holocene glacier reconstruction reveals retreat behind present limits and two-stage Little Ice Age on subantarctic South Georgia. *Journal of Quaternary Science* 32: 888-901.

van der Wal W, Whitehouse PL and Schrama EJO. (2015) Effect of GIA models with 3D composite mantle viscosity on GRACE mass balance estimates for Antarctica. *Earth and Planetary Science Letters* 414: 134-143.

Varma V, Prange M, Merkel U, Kleinen T, Lohmann G, Pfeiffer M, et al. (2012) Holocene evolution of the Southern Hemisphere westerly winds in transient simulations with global climate models. *Climate of the Past* 8: 391-402.

Vaughan DG, Marshall G, Connolley WM, Parkinson C, Mulvaney R, Hodgson DA, et al. (2003) Recent rapid regional climate warming on the Antarctic Peninsula. *Climatic Change* 60: 243-274.

Verfaillie D, Charton J, Schimmelpfennig I, Stroebele Z, Jomelli V, Bétard F, et al. (2021) Evolution of the Cook Ice Cap (Kerguelen Islands) between the last centuries and 2100 ce based on cosmogenic dating and glacio-climatic modelling. *Antarctic Science* 33: 301-317.

Verleyen E, Tavernier I, Hodgson DA, Whitehouse PL, Kudoh S, Imura S, et al. (2017) Ice sheet retreat and glacio-isostatic adjustment in Lützow-Holm Bay, East Antarctica. *Quaternary Science Reviews* 169: 85-98.

Wang G and Cai W. (2013) Climate-change impact on the 20th-century relationship between the Southern Annular Mode and global mean temperature. *Scientific Reports* 3: 2039.

Watcham EP, Bentley MJ, Hodgson DA, Roberts SJ, Fretwell PT, Lloyd JM, et al. (2011) A new Holocene relative sea level curve for the South Shetland Islands, Antarctica. *Quaternary Science Reviews* 30: 3152-3170.

Weatherall P, Marks KM, Jakobsson M, Schmitt T, Tani S, Arndt JE, et al. (2015) A new digital bathymetric model of the world's oceans. *Earth and Space Science* 2: 331-345.

Whitehouse PL, Bentley MJ and Le Brocq AM. (2012a) A deglacial model for Antarctica: geological constraints and glaciological modelling as a basis for a new model of Antarctic glacial isostatic adjustment. *Quaternary Science Reviews* 32: 1-24.

Whitehouse PL, Bentley MJ, Milne GA, King MA and Thomas ID. (2012b) A new glacial isostatic adjustment model for Antarctica: calibrated and tested using observations of relative sea-level change and present-day uplift rates. *Geophysical Journal International* 190: 1464-1482.

Yang L, Gao Y, Sun L, Xie Z, Yang W, Chu Z, et al. (2019) Enhanced westerlies drove penguin movement at 1000 yr BP on Ardley Island, west Antarctic Peninsula. *Quaternary Science Reviews* 214: 44-53.

Yoon H-I, Khim B-K, Lee K, Park Y-H and Yoo K-C. (2006) Reconstruction of postglacial paleoproductivity in Long Lake, King George Island, West Antarctica. *Polish Polar Research* 7: 189-206.

Zurbuchen J and Simms AR. (2019) Late Holocene ice-mass changes recorded in a relative sea-level record from Joinville Island, Antarctica. *Geology* 47: 1064-1068.